

Review

Open Access



Photothermal effect and application of photothermal materials in photocatalysis and photoelectric catalysis

Jingnan Zhang¹, Tongxin Tang², Rongge Yang¹, Guilin Wang², Kai-Hang Ye², Jianxin Shi¹

¹School of Chemistry, Sun Yat-sen University, Guangzhou 510275, Guangdong, China.

²Institute for Sustainable Transformation, School of Chemical Engineering and Light Industry, Guangdong University of Technology, Guangzhou 510006, Guangdong China.

Correspondence to: Prof. Kai-Hang Ye, Institute for Sustainable Transformation, School of Chemical Engineering and Light Industry, Guangdong University of Technology, No. 100, Waihuan West Road, Panyu District, Guangzhou 510275, Guangdong, China. E-mail: yekh@gdut.edu.cn; Prof. Jianxin Shi, School of Chemistry, Sun Yat-sen University, No. 132, Waihuan East Road, Panyu District, Guangzhou 510275, Guangdong, China. E-mail: cessjx@mail.sysu.edu.cn

How to cite this article: Zhang J, Tang T, Yang R, Wang G, Ye KH, Shi J. Photothermal effect and application of photothermal materials in photocatalysis and photoelectric catalysis. *Microstructures* 2024;4:2024008. <https://dx.doi.org/10.20517/microstructures.2023.51>

Received: 22 Sep 2023 **First Decision:** 16 Oct 2023 **Revised:** 26 Oct 2023 **Accepted:** 1 Nov 2023 **Published:** 18 Jan 2024

Academic Editors: Lianzhou Wang, Zhanxi Fan **Copy Editor:** Fangyuan Liu **Production Editor:** Fangyuan Liu

Abstract

Photocatalysis (PC) and photoelectric catalysis (PEC) are environmental protection technologies that use sunlight capacity and environmental governance, and they have a wide range of applications in hydrogen production, carbon dioxide reduction, organic degradation, and other fields. When the light is irradiated on the material, part of the light energy will be converted into heat energy, and the combination of this part of the heat energy with PC and PEC will become an important way to improve optical performance. Compared with traditional technology, the synergistic effect of light and heat can obtain higher catalytic performance and improve energy utilization efficiency. This review begins with an overview of the principle of photoheat generation, which produces heat energy in a non-radiative process through photo-induced instability of electrons. The principle of thermal effect on the performance improvement of PC/PEC is analyzed from the dynamics and thermodynamics of photoreaction and electric reaction. On this basis, several materials widely used at present are listed, such as oxides, plasmas, conductive polymers, carbon materials, and other typical photothermal materials. The specific applications of photothermal materials in PC and PEC processes, such as hydrogen production by oxidation, carbon dioxide reduction, organic matter reduction, and seawater desalination, were discussed. Finally, the challenges to PC/PEC from the introduction of thermal effects are further discussed to provide a clean and sustainable way to build a carbon-neutral society.

Keywords: Photothermal effect, photocatalysis, photoelectric catalysis, hydrogen production, carbon dioxide reduction



© The Author(s) 2024. **Open Access** This article is licensed under a Creative Commons Attribution 4.0 International License (<https://creativecommons.org/licenses/by/4.0/>), which permits unrestricted use, sharing, adaptation, distribution and reproduction in any medium or format, for any purpose, even commercially, as long as you give appropriate credit to the original author(s) and the source, provide a link to the Creative Commons license, and indicate if changes were made.



INTRODUCTION

With the development of the world economy and the increase of population density, the world is facing two major crises: one is energy demand, and the other is environmental pollution^[1-3]. To develop sustainable green energy instead of traditional fossil energy becomes an effective way to solve the energy crisis^[4-6]. At the same time, reducing carbon dioxide emissions through efficient and energy-saving ways can also effectively mitigate environmental pollution^[7,8]. Solar energy is the most abundant renewable energy on earth. The utilization of solar energy by photosynthesis in nature provides a solution for us. A shift from fossil fuels to clean energy, such as hydrogen, could significantly reduce carbon dioxide emissions^[9,10]. In 1972, Fujishima and Honda first proposed to use TiO₂ as photoanodes for water splitting^[11]. Using the energy level transition of semiconductors under sunlight to decompose aquatic hydrogen or reduce carbon dioxide has become an efficient means of solar energy conversion. Common semiconductor materials include TiO₂^[12], WO₂^[13], BiVO₄^[14], Fe₂O₃^[15], Cu₂O^[16], ZnO^[17], *etc.* All of them have different performance characteristics in photocatalysis (PC)/photoelectric catalysis (PEC).

The process of photocatalytic reactions is to excite electrons from the valence band (VB) to the conduction band (CB) by using the excitation of light on the semiconductor material to form an electron-hole pair^[18]. On this basis, PC promotes the separation of electrons and holes through applied voltage^[19]. The activity of photogenerated charge carriers is largely determined by the thermodynamics and kinetics of semiconductor materials^[20]. In thermodynamics, the photoexcitation makes the chemical potential of the electron system higher than that of the hole system, making ΔG negative, thus generating the photovoltage^[21-23]. In terms of dynamics, defects and doped atoms in semiconductor materials can act as charge transfer carriers to accelerate electron transport and may also act as charge aggregation centers to affect the recombination rate of electron holes^[24-26]. The current modification techniques mainly focus on the structure of the material itself, including band gap doping^[27], building nanostructures^[28], loading cocatalysts^[29], building composite heterostructures^[30], and other strategies. The principle of its modification is to accelerate the reaction kinetics and reduce the thermodynamic electromotive force, thus inhibiting the surface recombination of electrons and holes, forming a higher photogenerated current, accelerating the catalytic reaction process, and improving the stability of the catalyst^[31,32].

However, the improvement of the material performance through structural modification alone has its limitations. Therefore, the researchers use other systems to enhance the catalytic performance^[33]. Several common systems reported today include dual electrodes^[34], photovoltaic photoelectrochemical (PV-PEC) systems^[35], and semiconductor-based physical effects such as photothermal^[36], pyroelectric^[37], ferroelectric^[38], and piezoelectric^[39] effects. Using the physical effects of the material itself is a more refined approach than other electrochemical water decomposition systems. In catalytic reactions, reducing and utilizing the heat loss of the reaction can better improve the utilization rate of the reaction, so the photothermal effect has become an important direction of research^[40-42].

Photothermal effects mean that after the material is irradiated by light, the photon energy interacts with the lattice, making the vibration intensified, thus increasing temperature^[43]. Under the photothermal effect, the semiconductor absorbs and concentrates heat from the photons, and the thermal energy generated by the photoexcitation can heat the local lattice and enhance the vibration of the phonons. Theoretically, raising the temperature will increase the collision probability of the active molecules, promoting the dynamic process of the thermodynamic uphill reaction^[44-46].

This paper reviews the application of photothermal effects in PC/PEC systems. Firstly, the principle of photothermal effects improving photocatalytic performance is discussed, along with an examination of various photothermal materials. Then, the paper separately explores the applications of photothermal materials in photocatalytic and photocatalytic systems. [Figure 1](#) shows the review process of the research progress of photothermal materials in this paper.

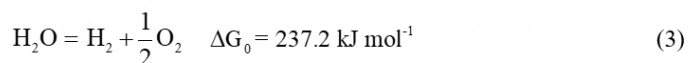
PRINCIPLE OF PHOTOTHERMAL EFFECT

The thermodynamics of PEC processes determine whether the reaction can proceed. The process of hydrogen production by PEC cracking water is to carry out redox reactions between the photogenic carrier generated by solar radiation on the catalyst surface or the active site of the catalyst and the solution to achieve hydrogen and oxygen production [[Figure 2A](#)]^[47,48]. In the research system of photoreaction, ultraviolet (UV) light is the main band of sunlight that acts on the photoexcitation of semiconductors. However, UV light accounts for only about 5% of the solar spectrum, and extending light absorption to the longer wavelength visible or even infrared light region can effectively use the energy of the spectrum. The visible light to infrared light region brings stronger photothermal effects in the process of PC^[49,50]. High utilization rates of light and good photothermal effects have become the consensus of improving energy conversion efficiency, but there are many different theories on the mechanism of photothermal effects on photocatalytic performance^[51].

As shown in [Figure 2B](#), the principle of photothermal effects can be analyzed from the molecular point of view. Photothermal materials make electrons enter the excited state by absorbing photons. In the excited state, electrons are unstable and undergo a series of deexcitation processes. In these processes, part of the non-radiative process will be converted into heat energy and emitted, that is, ultimately manifested as the process of converting light energy into heat energy^[52-54].

Effect of temperature on equilibrium and rate of chemical reaction

Water splitting as the content of photocatalytic reactions is analyzed. One molecule of H₂O can be converted to H₂ and 1/2 O₂ in the following reaction:



Therefore, PC is a typical energy uphill reaction, which needs to absorb heat. Based on the analysis of the basic physicochemical mechanism, the temperature adjustment can facilitate the equilibrium movement of chemical reactions, thus regulating the water decomposition performance of PEC^[55-57].

In 1884, Van't Hoff proposed the relationship between the equilibrium constant K of a chemical reaction and the change of temperature T in the Van't Hoff equation^[58]:

$$\frac{d \ln K}{dT} = \frac{\Delta H^\ominus}{RT^2} \quad (4)$$

(K is the equilibrium constant, ΔH is the enthalpy change, R is the gas constant, and T is the temperature).

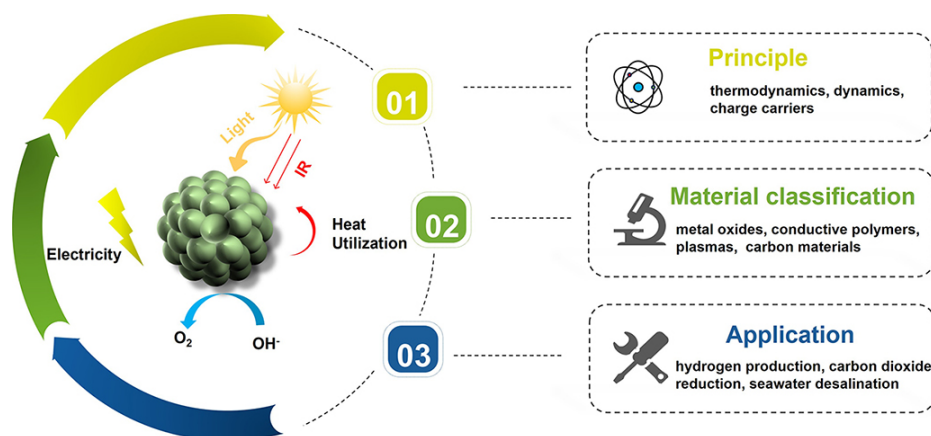


Figure 1. Current research progress of photothermal materials.

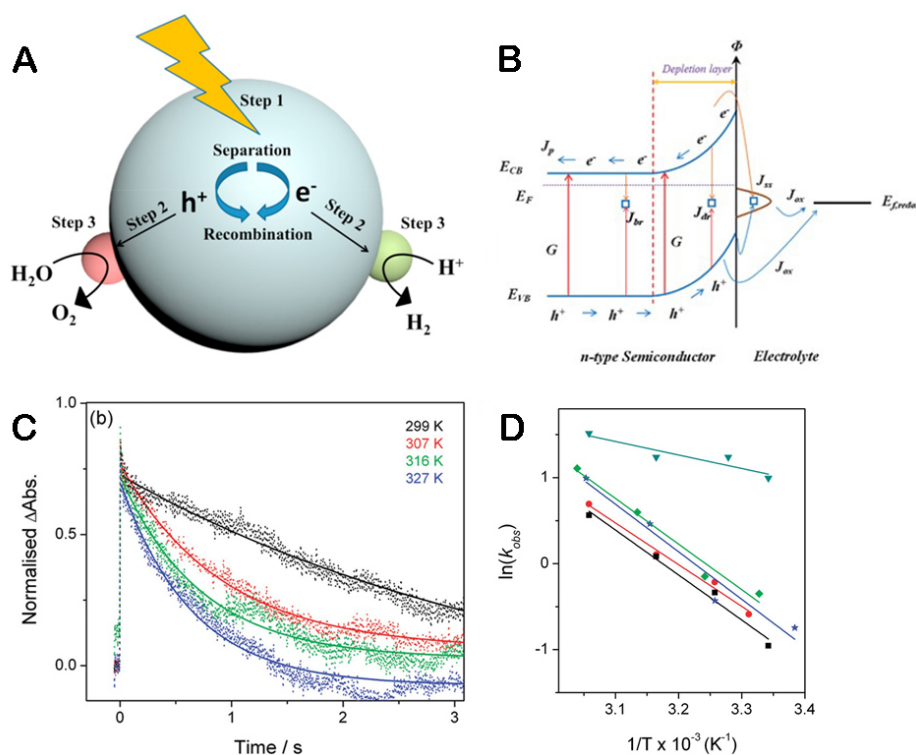


Figure 2. (A) The illustration of PEC water splitting using a photoanode^[53]. Copyright 2022, Elsevier Ltd. (B) The main recombination paths of semiconductor photogenerated holes and electrons^[57]. Copyright 2013, Royal Society of Chemistry. (C) TAS decay traces of the photohole in α -Fe₂O₃ photoanodes at different temperatures fitted to single-exponential functions. (D) Arrhenius plots of the hole decay on α -Fe₂O₃ photoanodes under various applied biases^[63]. Copyright 2011, American Chemical Society.

It can be seen from the equation that for endothermic reactions, with the increase of temperature, PEC reactions will move in the positive direction, thus producing more hydrogen and oxygen.

In several reaction steps of PC processes, the oxygen evolution reaction (OER) is the slowest and rate-determining step (RDS) in the water splitting reaction^[59,60]. From the relationship between the most basic chemical reaction rate and temperature, it can be inferred that temperature improves the catalytic reaction

process. The Arrhenius formula shows the relationship between the chemical reaction rate constant and temperature^[61]:

$$k = Ae^{-\frac{E_a}{RT}} \quad (5)$$

(k is the rate constant, R is the molar gas constant, T is the thermodynamic temperature, E_a is the apparent activation energy, and A is the pre-factor).

It can be seen from the equation that the pre-factor A determines whether the molecules collide in the right direction and only decides whether the reaction can proceed. The index $e^{-\frac{E_a}{RT}}$ determines the speed of the chemical reaction under the conditions under which the reaction occurs. With the increase of temperature, the reaction rate of OER processes is enhanced, and the performance of PEC is further improved^[62].

Cowan *et al.* used transient absorption spectroscopy (TAS) to investigate the temperature-dependent decay of photoluminescence holes in α -Fe₂O₃ during PEC^[63]. As shown in [Figure 2C](#), the photogenerated hole decay rate of α -Fe₂O₃ increases with rising temperature. The decay rate of photoluminescence holes is positively correlated with temperature under different bias pressures [[Figure 2D](#)].

Influence of thermal effects on electrochemical processes

A PEC process is characterized by light-electrochemistry interactions under an applied light that generates electron excitation following charge transfer from photoexcited materials. Therefore, it can be used as an electrochemical reaction, and its reaction process can be analyzed by an electrochemical reaction equation^[64]. The Nernst equation is used to describe the quantitative relationship between the electromotive force (E) electrolyte concentration of a battery. For the electrochemical process of water decomposition, the Nernst's equation can be written as^[65]:

$$E = E^0 + \frac{\Delta S}{nF}(T - T_0) - \frac{RT}{nF} \ln\left(\frac{a_{\text{H}_2} a_{\text{O}_2}^{1/2}}{a_{\text{H}_2\text{O}}}\right) \quad (6)$$

From $\Delta G_0 = 237.2 \text{ kJ mol}^{-1}$ of the water splitting reaction, the corresponding PEC initial potential (E_{cell}) should be -1.23 V according to the Nernst equation^[55]. When the temperature of the reaction system increases, the initial potential of PEC decreases. Under the same light and bias conditions, it is more conducive to the movement of charge and promotes the catalytic reaction^[66,67].

The paper of Ye analyzed the effect of temperature on the PEC performance of α -Fe₂O₃ photoanodes in water^[68]. As shown in [Figure 3A](#), the dark current density of α -Fe₂O₃ photoanode shifts at different temperatures. [Figure 3B](#) shows the temperature dependence of the starting potential of the electrode under light, and the starting potential is anodized with increasing temperature and decreasing doping level.

Temperature effect of band gap width of semiconductor materials

At present, the widely used photocatalysts are essentially semiconductors. Semiconductor materials have a fixed band gap energy (E_g), and the band gap energy width is determined by the energy level of the VB and the CB, that is, the energy difference between the lowest point of the CB and the highest point of the VB^[69]. In order to achieve water splitting to produce hydrogen and oxygen through PEC, the lowest potential of CB should be lower than the reduction potential of hydrogen ($\leq 0.0 \text{ V vs. RHE}$), and the highest potential of VB should be higher than the oxidation potential of oxygen ($\geq 1.23 \text{ V vs. RHE}$)^[70,71]. When a specific

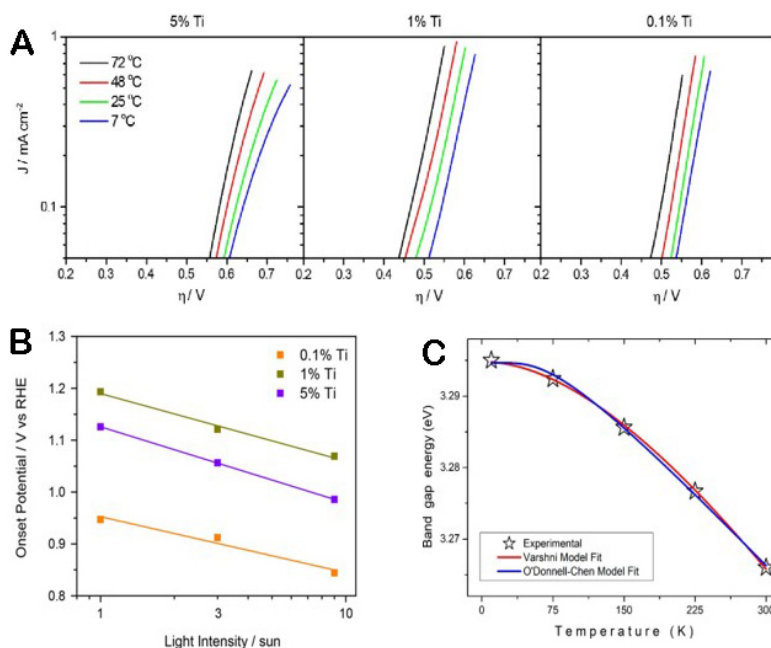


Figure 3. (A) The dark current density of hematite photoanodes with different temperatures. (B) Onset potential of a hematite photoanode as a function of the illuminated light intensity^[68]. Copyright 2016, Stanford University (C) Temperature-dependent band gap energy diagram of a TiO_2 photoelectrode^[69]. Copyright 2023, Springer Nature.

wavelength of light is irradiated on the catalyst, the absorption capacity of the PEC material is equal to or greater than the band gap energy of the semiconductor comprising the photoelectrode, which excites the electrons in VB to migrate to CB, correspondingly leaving a hole in VB to produce an electron-hole pair^[67].

The Varshni's equation can describe the band gap change of a semiconductor with temperature, and its equation form is as follows^[72]:

$$E_g(T) = E_g(0) - \frac{\alpha T^2}{T + \beta} \quad (7)$$

($E_g(T)$ is the band gap at temperature T , and α and β are the property constants of semiconductor materials).

According to the equation theory, the basic trend of material band gap with temperature change is as follows: as temperature increases, the band gap width of the material narrows^[73]. Figure 3C shows the spectrum diagram of the TiO_2 band gap width changing with temperature. As temperature increases, the band gap energy decreases^[69].

Combined with literature analysis, the reasons for the band gap change of a semiconductor with temperature can be analyzed from two aspects: first, the increase of temperature and the expansion of the lattice inside the material. The second is that the temperature increases and the lattice vibration intensifies, resulting in a stronger interaction between the phonons and electrons in the semiconductor^[74-76].

Temperature increases the carrier concentration in the semiconductor

The performance of photocatalysts is determined by three aspects: light absorption capacity, carrier separation efficiency, and carrier migration to the electrolyte/electrode interface. The carrier concentration plays an important role in increasing the rate of PC^[77-79]. It can be seen in [Figure 4A](#) and [B](#) that when the temperature increases, the band gap width of the semiconductor becomes smaller, and the photoelectrode can generate more intrinsic carriers under the same photoexcitation condition. In addition, the increase in temperature can also benefit the charge transport efficiency in the electrode and promote the separation of electron-hole pairs^[80-82]. In common photocatalysts, such as TiO₂, BiVO₄, WO₃, and Fe₂O₃, the minority carriers are usually small polarons that are easily trapped, and an appropriate increase in temperature can activate the minority carrier transition of the semiconductor[[Figure 4C](#)]^[83].

In their study on the temperature characteristics of BiVO₄ photoanodes, Zhou *et al.* conducted electrochemical impedance spectroscopy (EIS) to investigate the interfacial charge transfer kinetics at different temperatures^[84]. As shown in [Figure 4D](#), the Nyquist diagram at various temperatures shows the correlation between the imaginary part ($\text{Im}Z(f)$) and the real part ($\text{Re}Z(f)$). From 23 °C to 35 °C, R_s decreased by more than 40%, indicating that the electronic conductivity of BiVO₄ increases with increasing temperature. At higher temperatures, the small polaron transition of BiVO₄ is activated, and more intrinsic carriers are generated, which promotes the increase of photocurrent.

CLASSIFICATION OF MATERIALS FOR PHOTOTHERMAL EFFECTS

Many materials exhibit photothermal effects, and currently, five common categories of photothermal materials are applied to PC/PEC. One is metal oxides, which include a range of spinel-structured materials. The second is metal sulfides, of which the selenides within the same family also demonstrate similar photothermal properties. Third, there are metal point materials, most of which manifest plasma effects. The fourth category comprises conductive polymers, mainly polyaniline (PANI) and polypyrrole. Fifth, all kinds of carbon-based materials, such as carbon quantum dots (CQDs), graphene, carbon nanotubes (CNTs), and so on, are included. In this section, the above five photothermal materials currently applied to PC/PEC are introduced as follows. [Figure 5](#) shows the main classification of photothermal materials.

Metal oxide

TiO₂, BiVO₄, and Fe₂O₃, which are commonly used as photocatalytic semiconductors in current research, have certain photothermal effects. Wang *et al.* synthesize a unique core-amorphous shell structure (TiO₂@TiO_{2-x}) by an aluminum reduction method, which improves visible and infrared light absorption through light collecting effects^[85]. After 60 s of simulated sunlight irradiation, the temperature of Black TiO_{2-x} rose to 37 °C compared to 28 °C for the original TiO₂. The accelerated heating rate of Black TiO_{2-x} is due to increased absorption of solar energy, increased electron excitation and relaxation, and enhanced thermal emission.

[Figure 6A](#) and [B](#) lists the study of Zhou *et al.* on the relationship between the BiVO₄ photoanode and temperature^[84]. The enhancement of its photothermal effect can be attributed to two factors. First, concerning the reversible aspect, small polarons in BiVO₄ are activated to promote the separation and transport of electron holes. Second, in terms of irreversibility, at high temperatures, the BiVO₄ photoanode interacts with a hole scavenger to form a stepped amorphous layer on the surface, which improves the separation of charge carriers.

Dias *et al.* find that the initial potential of Si-mixed Fe₂O₃ changes with the increase of temperature, and the optimal initial potential is reached at 45 °C^[86]. Ye *et al.* studied the effect of temperature on Ti-mixed

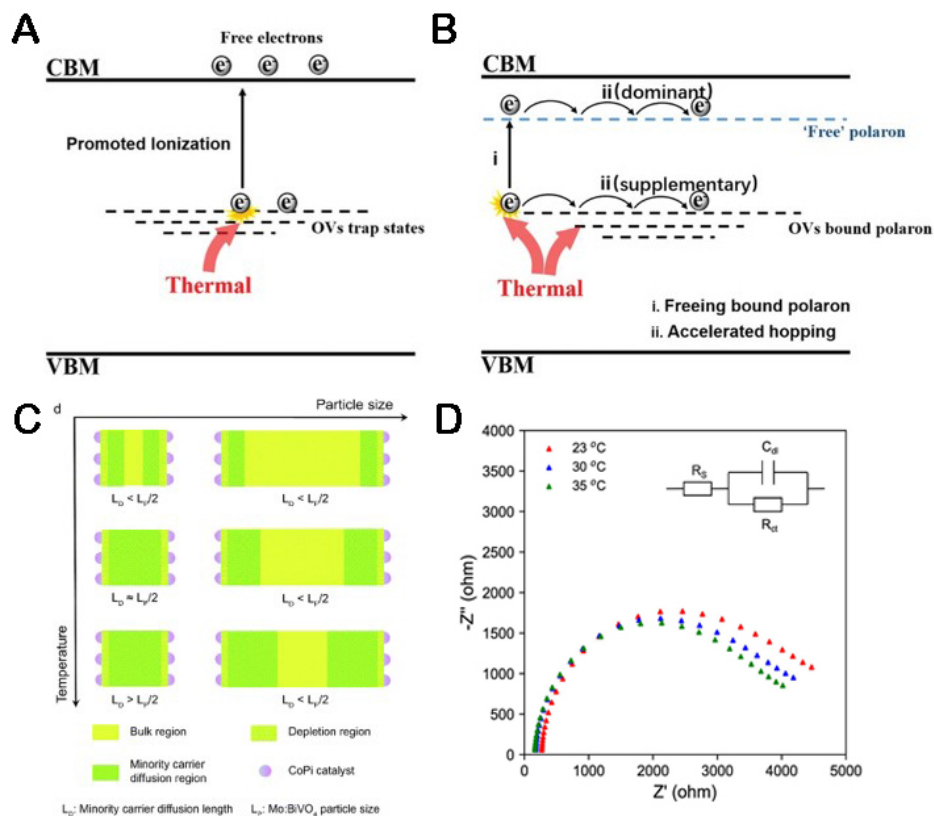


Figure 4. (A) Thermally improved doping efficiency. (B) Thermally activated bound polaron hopping^[83]. Copyright 2022, John Wiley & Sons, Inc. (C) A schematic illustration of the relationship between minority carrier diffusion length (L_D) and particle size (L_p) as a function of temperature^[82]. Copyright 2016, Royal Society of Chemistry. (D) Nyquist plot of BiVO₄ measured at 1.2 V_{RHE} at different temperatures^[84]. Copyright 2021, American Chemical Society.

Fe₂O₃^[87]. When the temperature increases, the required potential to reach saturation photocurrent decreases [Figure 6C]^[87].

In addition to the photothermal effect of the photocatalyst itself, cobalt oxide can make the temperature rise rapidly under infrared irradiation in the loaded mixed metal oxide. He *et al.* place the photothermal material Co₃O₄ as a sandwich between the BiVO₄ photoanode film and the FeOOH/NiOOH electrocatalyst sheet^[88]. When irradiated by 808 nm near-infrared light, the temperature of Co₃O₄ rapidly rose from 296.15 K to 333.15 K within 60 s, showing a strong photothermal effect. Zhang *et al.* use scanning photoelectrochemical microscopy (SPECM) to analyze the photoluminescence of BiVO₄/CoO_x [Figure 7A]^[89]. Under light, as the substrate temperature increased, the probe current showed a positive correlation [Figure 7B], during which temporal holes accumulated on the surface of the photoanode and participated in the oxidation process [Figure 7C].

Some metal oxides with spinel structures also have photothermal properties and are used in photocatalytic hybrid materials. He *et al.* studied spinel-type MCo₂O₄ oxide (M = Ni, Mn, Zn, Cu, and Fe) materials and designed NiCo₂O₄ (NCO)/BiVO₄ photoanodes^[90]. With the help of photothermal effects, the photocurrent density of the photoanode was 6.20 mA cm⁻² at 1.23 V reversible hydrogen electrodes. The oxides of spinel structures absorb light and heat energy under infrared irradiation by virtue of their photothermal properties. The band bending at the interface between photothermal catalysts and photocatalysts is increased, which is conducive to the transfer of holes to MCo₂O₄.

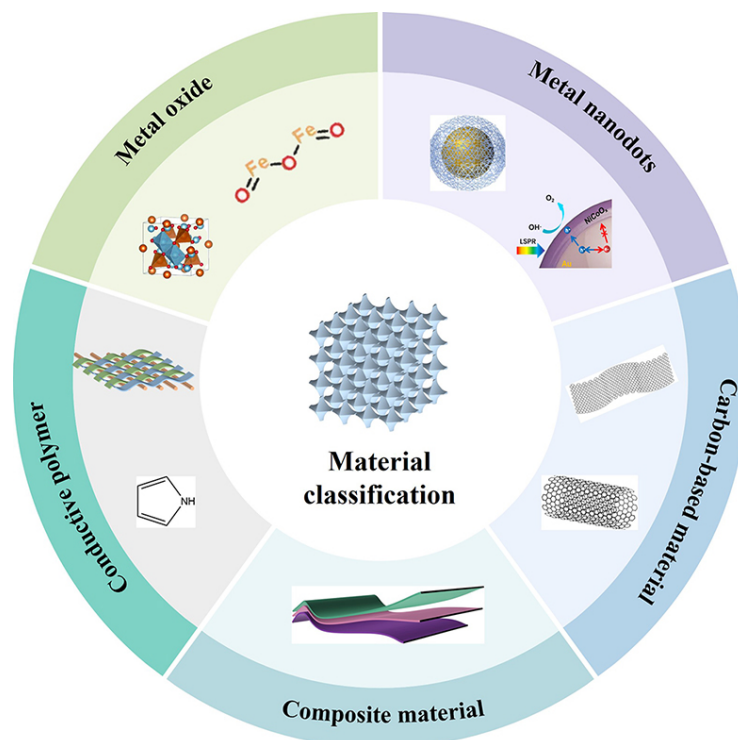


Figure 5. Main classification of photothermal materials.

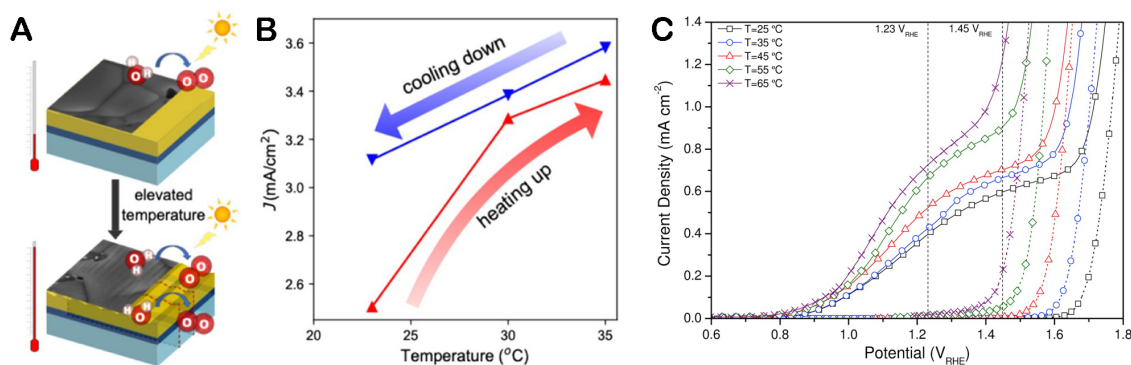


Figure 6. (A) Schematic diagram of improvement of charge transfer with temperature increase. (B) The change of photocurrent density of BiVO_4 with temperature^[84]. Copyright 2021, American Chemical Society. (C) Photocurrent density-voltage (J - V) characteristics of Si-doped $\alpha\text{-Fe}_2\text{O}_3$ photoelectrodes at different temperatures^[86]. Copyright 2014, Elsevier Ltd.

Huang *et al.* use spinel oxide NCO as a photothermal material to assist TiO_2 photoanodes to enhance their PEC performance^[91]. NCO/ TiO_2 obtained a photocurrent of 2.34 mA cm^{-2} at $1.23 V_{\text{RHE}}$. The dynamic oxidation of Ni^{2+} in NCO catalysts was tracked by cyclic voltammetry (CV). As shown in Figure 7D, the oxidation peak of Ni^{2+} to Ni^{3+} transformation is between 1.3-1.4 V, and under the irradiation of near-infrared light, the oxidation peak potential continues to move downward. The results indicate that the photothermal conversion can promote the pre-oxidation of Ni^{2+} , which is conducive to the subsequent formation and catalytic reaction of Ni-OOH. In addition, as analyzed by EIS, NCO showed an earlier transition peak at a lower potential of $1.45 V_{\text{RHE}}$ under near-infrared light, which may be due to the photothermal effect that promotes faster deprotonation of $^*\text{OOH}$ [Figure 7E and F].

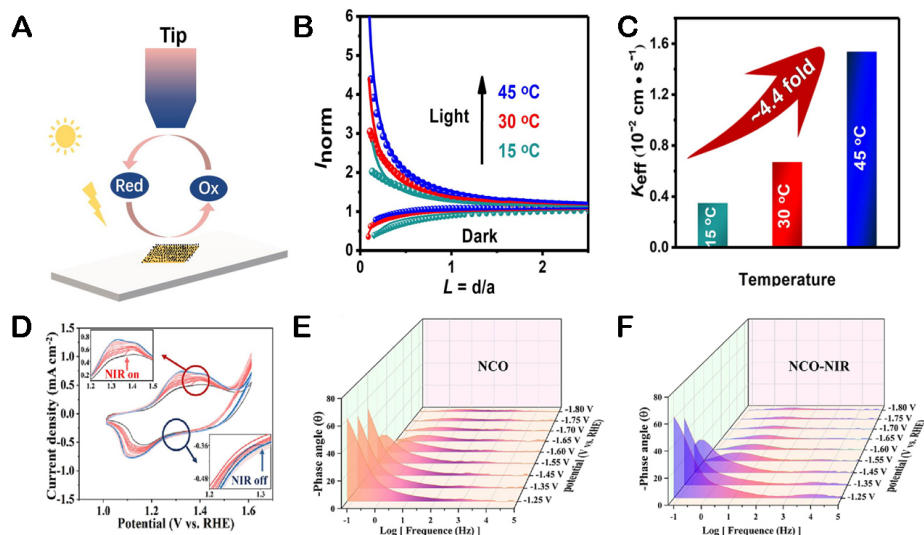


Figure 7. (A) Principle of the SPECM setup. (B) Probe current curve with temperature. (C) Rate constants (K_{eff}) of composite photoanodes at different temperatures^[89]. Copyright 2021, Academic Press Inc Elsevier Sci. (D) The change of CV curves for the NCO electrode under NIR on and NIR off conditions. (E) EIS-derived Bode plots of NCO. (F) EIS-derived Bode plots of NCO-NIR^[91]. Copyright 2023, Elsevier Sci.

Hu *et al.* deposit ZnFe_2O_4 nanoparticles (NPs) on the surface of Fe_2O_3 and the charged small poles generated by the photothermal effect of ZnFe_2O_4 combined with the positively charged oxygen vacancy^[92]. The synergistic effect between the photothermal effect and the oxygen vacancy improved the performance of PEC.

As the first reported photothermal material in PEC, the current research mainly focuses on the oxides containing Co and Fe elements, whose advantages are relatively low price, and as a semiconductor material itself, it can improve the performance of PEC even without heating.

Metal sulfide and metal selenide

Sulfides also have a certain photothermal effect, and the most common sulfides are mainly Cu_2S , Bi_2S_3 , MoS_2 , and so on^[93]. Zhang *et al.* constructed $\text{Cu}_2\text{S}/\text{Fe}_2\text{O}_3$ heterojunction photocatalysts and improved their PEC performance by utilizing the heterojunction and photothermal effects^[94]. The formation of S-O bonds at the heterogeneous interface of Cu_2S and Fe_2O_3 makes contact tighter and reduces the interface contact resistance, thus promoting charge transfer and improving stability. In addition, Cu_2S itself has high photothermal properties, and its photothermal effect makes the heterojunction electrode reach a local high temperature under light, which is conducive to accelerating the OER rate^[95].

Zhao *et al.* deposit the narrow band gap semiconductor Bi_2S_3 on the surface of WO_3 nanosheets^[96]. Using the photothermal conversion characteristics of Bi_2S_3 , the photocurrent density of $\text{Bi}_2\text{S}_3/\text{WO}_3$ composite photoanodes to the reversible reference electrode reaches 4.05 mA cm^{-2} at 1.23 V (V_{RHE}). An EIS Nyquist test was performed on the material to analyze its photothermal effect. The fitting values extracted from the Nyquist diagram are listed in Table 1. The R_{bulk} value of $\text{PI-WO}_3/\text{Bi}_2\text{S}_3$ (25.97Ω) is smaller than that of $\text{WO}_3/\text{Bi}_2\text{S}_3$ (43.61Ω), and the surface photothermal effect enhances charge transfer.

In addition, some ternary sulfides, CdSeS , ZnInS , and ZnCdS , which have similar spinel structures, have also been applied to photothermal PEC processes^[97-99].

Table 1. Fitting results of R_s , R_{bulk} , and R_{int} for different samples by ZVIEW^[96]

Photoanodes	R_s (Ω)	R_{bulk} (Ω)	R_{int} (Ω)
WO ₃	25.60	57.58	5,713
PI- WO ₃	25.36	53.68	4,890
Bi ₂ S ₃ /WO ₃	25.62	43.61	2,905
PI- Bi ₂ S ₃ /WO ₃	25.20	25.97	1,898

As a congener of sulfides, selenides have similar properties, but there is currently limited research on metal selenides used in photothermal applications. Li *et al.* prepared MoSe₂-CDs-ZnO (M2CZ2), in which MoSe₂ nanosheets strongly absorb light at the full spectrum (from UV to near-infrared) and can be used as the main photothermal materials^[100]. The hydrogen production of M2CZ2 was investigated under the condition of a water bath. After heating for 4 h, the H₂ precipitation of M2CZ2 reached 158.6 $\mu\text{mol cm}^{-2}$. As shown in **Figure 8A**, after 2 min irradiation, M2CZ2 increased by about 32 °C, indicating a significant temperature rise, while the control group only increased by 15 °C. **Figure 8B** shows the temperature changes of different electrodes in electrolytes under the irradiation of 300 W Xe lamps. M2CZ2 increases by 20 °C, which proves that it can also significantly increase temperature in PEC systems. The reaction hydrogen production process and thermal imaging diagram are shown in **Figure 8C** and **D**.

As S and Se are in the same family as O, the properties of sulfides and selenides themselves have many similarities with oxides. However, due to the fact that the synthesis of sulfide (selenide) itself produces toxic gases, such as hydrogen sulfide, and the cost is relatively higher, there are few literature studies on these two types of materials.

Metal nanodots

Among many photothermal materials, metal nanodot materials have their unique photothermal properties, that is, the local surface plasmon resonance effect (LSPR) of metal NPs^[101,102]. The size of the metal NPs is smaller than the wavelength of the incident light, and the free electrons on the surface of the conductive material are excited and oscillate^[103]. When the electron vibration frequency matches the incident light frequency, the metal NPs will produce strong absorption of the photon energy, resulting in resonance effects, which will stimulate the production of hot electrons [**Figure 9**]^[103-105].

Plasma materials require good chemical stability and high stability. Among them, Au NPs, as plasma materials, have been widely studied for PEC^[106,107]. Tang *et al.* deposited NiCoO_x electrocatalytic layers on the surface of Au NPs^[108]. Due to the LSPR and photothermal effect of plasma Au NPs, the current density of NiCoO_x/Au anode increased by 7.01 mA cm⁻² under light. **Figure 10A** and **B** shows optical simulations of Au NPs and NiCoO_x separated Au NPs at an excitation wavelength of 550 nm. The edge of the Au NPs in the two images forms a strong spatial non-uniform oscillating electric field, which is a characteristic of the LSPR effect. Agarwal *et al.* use a silicon material as the inner core of the Au-loaded plasma film (Au-coated Si nanowire)^[109]. The use of a semiconductor metal nanowire cavity to enhance the plasma properties of the Au NPs results in the resonance of intense heat [**Figure 10C**]. Under light conditions, the temperature in the nanowire cavity reaches ~1,000 K, which increases the H₂ formation rate of ethanol photoreforming reactions by about 40%. Zhang *et al.* deposited 20 nm Au NPs on the nanotube array of TiO₂ and used the hot electrons generated by the LSPR effect of Au to inject the conduction band of TiO₂, resulting in a photocurrent density of about 150 $\mu\text{A cm}^{-2}$ under visible light^[106].

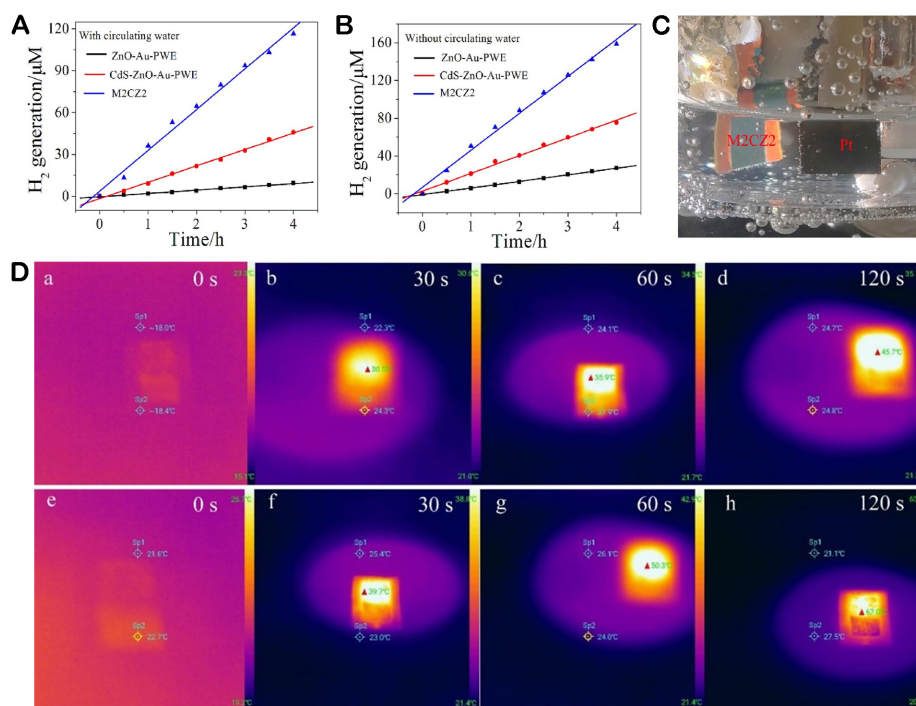


Figure 8. (A) Photocatalytic hydrogen production at a photoelectrode with water bath heating at 0 V (vs. Ag/AgCl). (B) Photocatalytic hydrogen production at a photoelectrode without water bath heating at 0 V (vs. Ag/AgCl). (C) H₂ generation on Pt counter electrodes with light irradiation. (D) Infrared thermal images of the CdS-ZnO-Au-PWE (a-d) and M2CZ2 (e-h) under different irradiation times of 300 W Xe lamps^[100]. Copyright 2021, Elsevier Ltd.

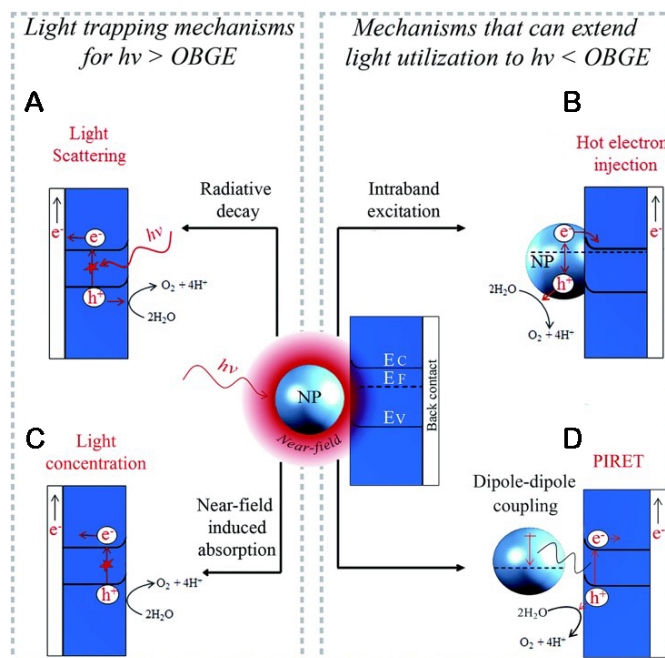


Figure 9. Four energy transfer mechanisms from a plasmonic NP to an n-type semiconductor to drive water oxidation: (A) light scattering, (B) hot electron injection, (C) light concentration, and (D) plasmon-induced resonance energy transfer (PIRET)^[104]. Copyright 2015, American Chemical Society.

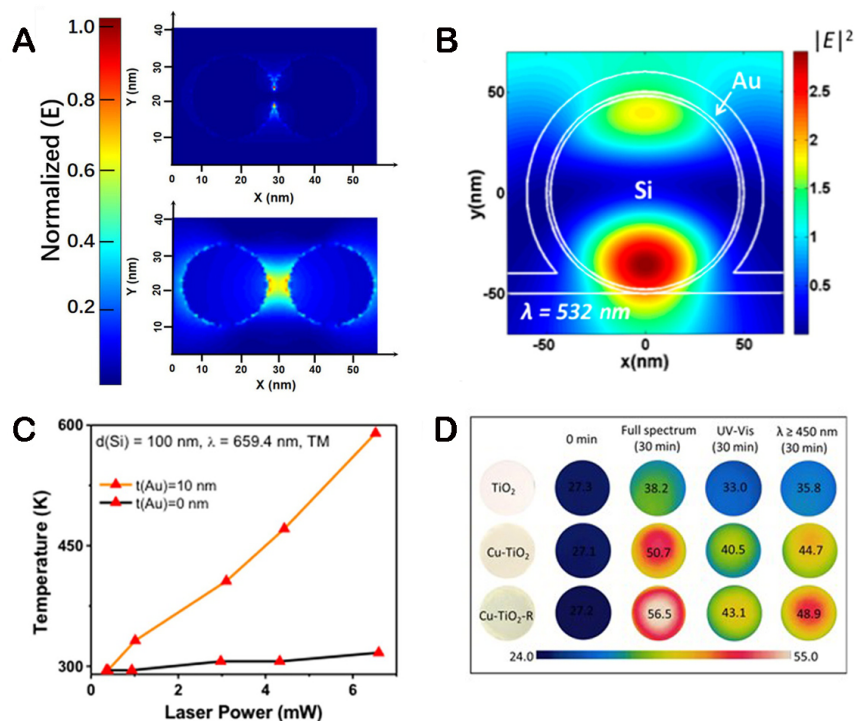


Figure 10. (A) Spatial normalized distribution of electric fields of gold nanoparticles (top) and NiCoO_x-separated gold nanoparticles (bottom). (B) Spatial distribution of electric field intensity inside the cavity under TM excitation for 10 nm Au-coated Si nanowire at 532 nm^[108]. Copyright 2023, John Wiley & Sons, Inc. (C) Temperature versus laser power for Au-coated and bare Si nanowires under TM polarization at 659.4 nm excitation^[109]. Copyright 2017, American Chemical Society. (D) Infrared images taken under both full-spectrum, UV light, and $\lambda \geq 450$ nm after irradiation for 30 mins of the TiO₂, Cu/TiO₂, and Cu/TiO₂-after reactions (Cu/TiO₂-R)^[114]. Copyright 2020, John Wiley & Sons, Inc.

The cost of Au is expensive, and metals Ag, Cu, Fe, Ni, Bi, and other NPs are also used as cost-effective materials^[110-113]. Song *et al.* prepare Cu/TiO₂ NPs, and the introduction of 3-6 nm Cu NPs significantly improved the photocatalytic hydrogen production rate of TiO₂^[114]. The photothermal effect of Cu NPs causes the local temperature of the catalyst surface to increase, which significantly reduces the activation energy of the reaction and improves the charge separation efficiency [Figure 10D]. Li *et al.* use a chemical reduction method to hybridize Cu NPs with TiO₂ *in situ*^[115]. Under the display of an infrared thermal imager, the temperature of Cu/TiO₂ composites can reach about 80 °C after 2 min of illumination, while the temperature rise of TiO₂ is not obvious. In the test of hydrogen production, the hydrogen production of Cu/TiO₂ gradually rises with the increase of temperature, and the hydrogen production rate is as high as 24,160.69 $\mu\text{mol g}^{-1} \text{h}^{-1}$ at 100 °C. This provides a low-cost and high-efficiency preparation method of noble-free photocatalysts for constructing photocatalytic materials. Subramanyam *et al.* add Bi NPs to the C₃N₄/Bi₂S₃ photoanode by a drip method, and the photocurrent density of the composite can reach 7.11 mA cm⁻²^[116]. The surface plasmon resonance (SPR) characteristics of Bi NPs improve the light absorption and charge carrier density, which is conducive to improving the PEC performance.

The photothermal effect of metal nanodots is largely derived from the plasmon resonance effect. At present, the application reports of metal nanodots are mainly concentrated in the field of PC. Among them, the photothermal effect of Au and Ag is better, but the corresponding cost and synthesis conditions are also elevated. At present, the research of Cu nanodots is more popular, and the investigation of other common metal nanodots needs to be further explored.

Conductive polymer

As an organic conductive material, conductive polymers are mainly based on hole transport, and it has been proved by experiments that they also have photothermal conversion effects, which can be applied in photothermal PEC^[117].

Zhao *et al.* constructed Co-Pi/PANI/BiVO₄ composite photoanodes with PANI and cobalt phosphate (Co-Pi) as cocatalysts^[118]. On the one hand, as a hole carrier, PANI and BiVO₄ form p-n heterojunction to enhance charge separation. On the other hand, the photothermal effect of PANI causes the temperature of the reaction electrode to rise, activates the minority carrier transition, and further improves the charge separation efficiency. A significant water oxidation photocurrent of 4.05 mA cm⁻² was obtained at 1.23 V_{RHE}, which is more than 300% higher than the original BiVO₄ photoanode [Figure 11A and B].

Xu *et al.* propose to use the conjugated polymer polypyridine (PPy) with high conductivity and good photothermal effects as a multifunctional surface modifier for the photoelectrochemical (PEC) water decomposition of terene metal sulfides (CdIn₂S₄, CIS)^[119]. The principle of near-infrared photoanodes applied to PEC water cracking is shown in Figure 11C. The introduction of Ni further accelerates the surface reaction kinetics, including the reduction of charge transfer resistance and the negative displacement of the plane band potential. In addition, PPy exhibits photothermal properties under near-infrared radiation, which can be targeted to improve the surface temperature of the photoanode material.

At present, the research literature on photothermal materials of conductive polymers is the scarcest compared with other types of materials, and the main field is focused on PEC. Conductive polymers inherently possess good electrical conductivity and light absorption effects, but the challenge lies in effectively combining conductive polymers with photoelectric materials. Therefore, they hold substantial development prospects in the future development of photothermal materials.

Carbon-based materials

In many studies, carbon-based materials are often used as carriers of electrocatalysts because of their large surface area and excellent charge mobility. The carbon-based material itself has a darker color, and it also has a good application prospect in the light absorption of photothermal conversion^[120-122].

CQDs, as typical carbon-based photothermal materials, can effectively convert the energy of near-infrared light into local heat and are the most widely used photothermal materials in carbon-based materials^[123]. Hu *et al.* prepared Co-Pi/CQDs/Fe₂O₃/TiO₂ photoelectrodes using Fe₂O₃/TiO₂ as the main photocatalyst material by combining CQDs and other materials^[124]. Under the irradiation of 808 nm near-infrared light, the platform temperature of Co-Pi/CQDs/Fe₂O₃/TiO₂ can reach 42 °C, indicating that CQDs have high photothermal conversion efficiency. At 1.23 V_{RHE}, the current density greatly increased as the electrolyte temperature rose, confirming the possibility of elevating the electrode operating temperature to improve the activity of the α-Fe₂O₃ photoanode.

Cai *et al.* prepare (Ti, Zn)-Fe₂O₃@Ti-Fe₂O₃@C&Co-Pi by means of heteroatomic mixing, in which CQDs are attached to Fe₂O₃ rods in the form of anchor points^[125]. CQDs produce local thermal effects under near-infrared irradiation; the photocurrent density increases to 1.02 mA cm², and the initial potential shifts by 0.87 V. The photothermal effect increases the contact potential difference and band bending at the semiconductor-electrolyte interface [Figure 12].

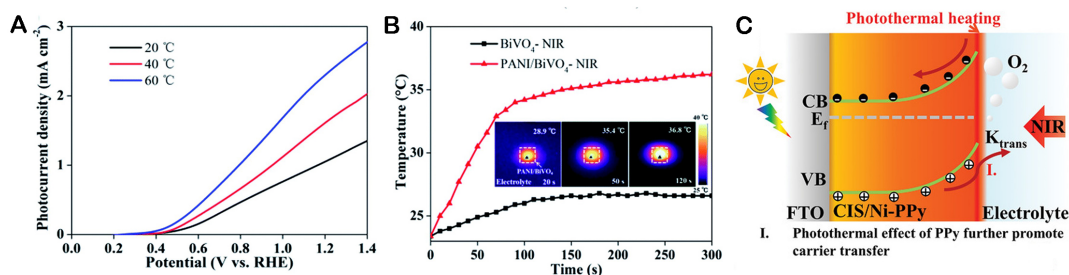


Figure 11. (A) Temperature-dependent photocurrent-voltage curves of the BiVO₄ photoanode. (B) Temperature-time plots of BiVO₄ and PANI/BiVO₄ with NIR light^[118]. Copyright 2020, Royal Society of Chemistry. (C) Schematic illustration of the band energy alignment of CIS/Ni-PPy + NIR photoanodes^[119]. Copyright 2022, John Wiley & Sons, Inc.

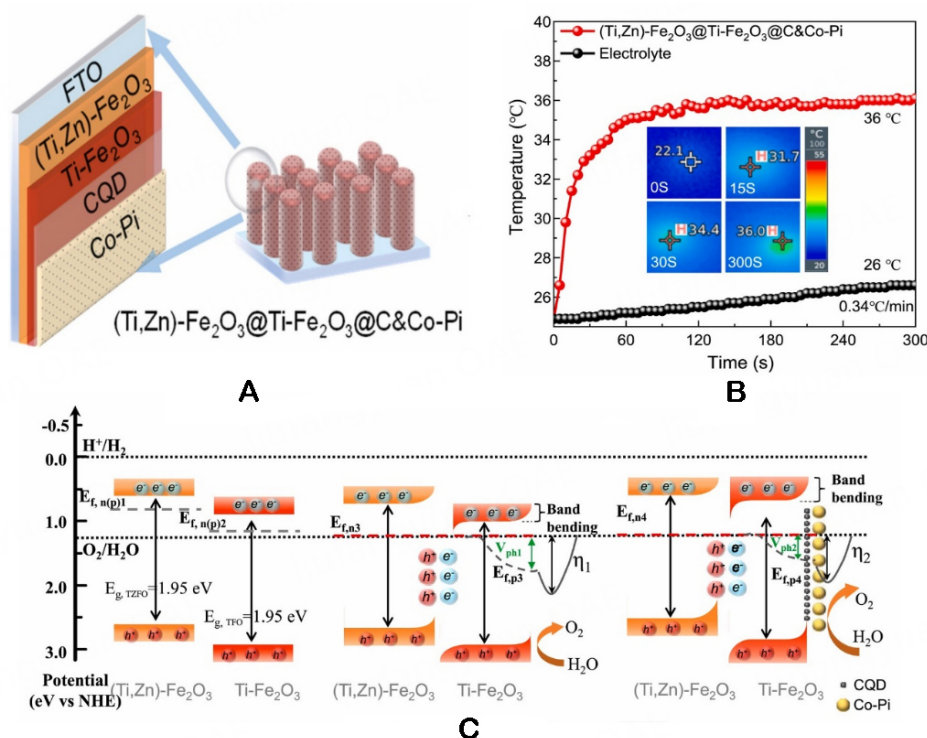


Figure 12. (A) The structure diagram of (Ti, Zn)-Fe₂O₃@Ti-Fe₂O₃@C&Co-Pi. (B) The temperature variation of the sample under 10 W illumination. (C) The band alignment of the sample under AM 1.5 and NIR illumination^[125]. Copyright 2023, Elsevier Ltd.

As a two-dimensional conductive material, the excellent electrical properties of graphene find frequent applications in photoelectric material composites^[126]. Wu *et al.* synthesize rGO/Na₂Ti₃O₇ nanospheres by a hydrothermal method [Figure 13A]^[127]. The coupling of layered Na₂Ti₃O₇ and rGO significantly improved the PEC properties under visible light irradiation. Under light irradiation, the rGO/Na₂Ti₃O₇ microsphere can act as a microheater, and the local temperature is significantly increased, making it much higher than the average solution temperature. This local thermal effect can effectively absorb the reactants and significantly accelerate the reaction kinetics. In addition, the electrons on the rGO sheet can gain extra energy to move quickly, inhibiting the recombination of electron holes.

In Figure 13B and C, Fang *et al.* synthesize g-C₃N₄ materials by a hard template method and study the hydrogen production rate of g-C₃N₄ under three ways of photothermal catalysis, PC, and thermal

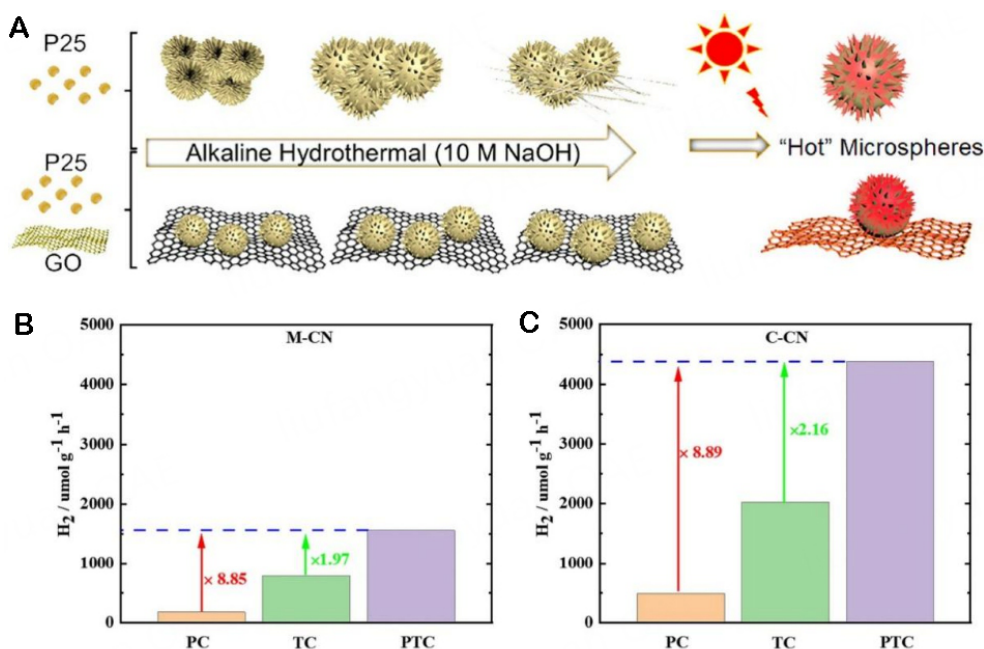


Figure 13. (A) Schematic diagram of the growth mechanism of $\text{Na}_2\text{Ti}_3\text{O}_7$ and $\text{rGO}/\text{Na}_2\text{Ti}_3\text{O}_7$ microspheres^[127]. Copyright 2020, American Chemical Society. (B) Hydrogen evolution rate over melamine (M-CN) via the TPC (80 °C), PC and TC (80 °C) pathways. (C) Hydrogen evolution rate over cyanamide (C-CN) via the TPC, PC and TC pathways^[128]. Copyright 2023, Elsevier Ltd.

catalysis^[128]. At 60 °C, the photothermal synergistic hydrogen production rate reaches $1,932.9 \mu\text{mol g}^{-1} \text{h}^{-1}$, which is much higher than that of thermal catalysis or PC alone. With the increase of temperature, the thermal catalytic performance of C_3N_4 is improved more obviously, which shows that C_3N_4 has a good photothermal conversion performance.

In addition, the photothermal properties of carbon hemispheres, three-dimensional CNTs, and carbonized melamine foam (C-MF) have also been reported^[129,130].

Other photothermal materials

In recent years, a variety of photothermal materials have appeared, such as organic matter, MXenes, elemental S, *etc.*, which can improve the photocatalytic performance by increasing the temperature of the photoelectrode.

As two-dimensional metal carbide materials, MXenes have many similarities with graphene in structures and properties. Under infrared irradiation, MXene materials can generate a lot of heat and increase the surface temperature of the photoanode. Xie *et al.* graft MXene nanosheets as surface modifiers onto ZnO nanorods^[131]. Under light, the temperature of MXene nanosheets rapidly increased from 17.8 °C to 35.7 °C [Figure 14A].

Zhang *et al.* constructed sulfur-mixed iron nickel-metal hydride oxide ($\text{S-NiFeO}_x\text{H}_y/\text{CC}$) on carbon cloth^[132]. As shown in Figure 14B, UPS tests show that the valence band of $\text{S-NiFeO}_x\text{H}_y/\text{CC}$ shifts towards Fermi level when sulfur is mixed, which makes $\text{S-NiFeO}_x\text{H}_y/\text{CC}$ have stronger light absorption performance for the full spectrum of sunlight. The surface temperature of $\text{S-NiFeO}_x\text{H}_y/\text{CC}$ increases rapidly under light, up to 82.6 °C [Figure 14C].

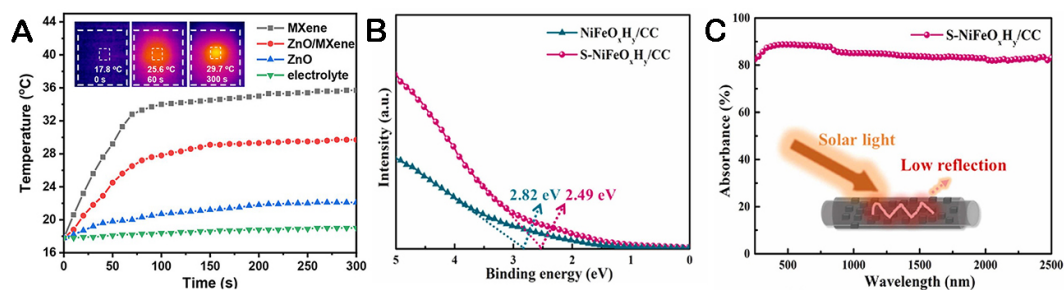


Figure 14. (A) Time-dependent temperature curves of the electrolyte ZnO/MXene nanorod arrays irradiated by 808 nm NIR light^[131]. Copyright 2022, American Chemical Society. (B) The UPS spectra of NiFeO_xH_y/CC and S-NiFeO_xH_y/CC. (C) The UV-vis-NIR absorption spectrum of S-NiFeO_xH_y/CC^[132]. Copyright 2023, Elsevier Ltd.

In addition, there are also researchers to develop various types of photothermal materials to harness synergistic effects.

Zhang *et al.* prepare a snowflake Cu₂S/MoS₂/Pt material by a hydrothermal method and electrodeposition^[133]. Under infrared induction, the photothermal effect of MoS₂ can generate a larger photocurrent by increasing the electron transfer speed and interface electrochemical reaction, and the LSPR effect of Pt NPs further stabilizes the photothermal properties of the material. At the same time, due to the special geometric and electronic structure of Cu₂S, it has a positive effect on hydrogen production by PEC.

Cao *et al.* constructed CQDs/Au/TiO₂ nanorod array composite photoanodes^[134]. The electric field of CQDs/Au/TiO₂ photoanodes was simulated by a finite element method. Due to the SPR effect, the electric field near Au is obviously enhanced. The coupling between Au and TiO₂ promotes the transfer of hot electrons to the semiconductor through the metal-semiconductor interface. The electric field inside CQDs is the smallest in the whole region, which plays the role of hole heat collection. The synergistic effect of Au and CQDs not only stimulates the small polaron transport activity of semiconductor TiO₂ but also accelerates the charge transfer and surface reaction from the aspects of kinetics and thermodynamics. The H₂ precipitation rate of CQDs/Au/TiO₂ photoanodes is five times that of blank TiO₂.

By electrodeposition and CV, Zhao *et al.* load Au NPs and rGO onto TiO₂ nanotube arrays, respectively, to prepare Au/rGO/TiO₂ photoelectrodes^[135]. COMSOL is used to simulate the temperature field of the photoelectrode. As shown in Figure 15A and B, due to the high thermal conductivity of rGO, the heat transfer of Au NPs to TiO₂ can be accelerated, so Au-rGO/TiO₂ can more fully transfer heat from the top of the nanoring to the nanotube. The synergistic effect between the thermal plasma effect of Au NPs and the excellent heat transfer performance of graphene oxide was confirmed.

APPLICATION OF PHOTOTHERMAL MATERIALS

The research of photothermal materials is not only limited to the mechanism of photothermal generation of the material itself but also fully applied to its photothermal properties in all directions. Through the combination of PC, solar cells, *etc.*, the performance of photothermal materials can be realized^[136-138]. The energy utilization rate can be improved, and the product conversion rate can be improved. Figure 16 shows the application areas of different photothermal materials.

PC and photothermal effect

Photothermal catalytic water decomposition

For photocatalytic water decomposition, the thermal energy converted by the full spectrum of sunlight can

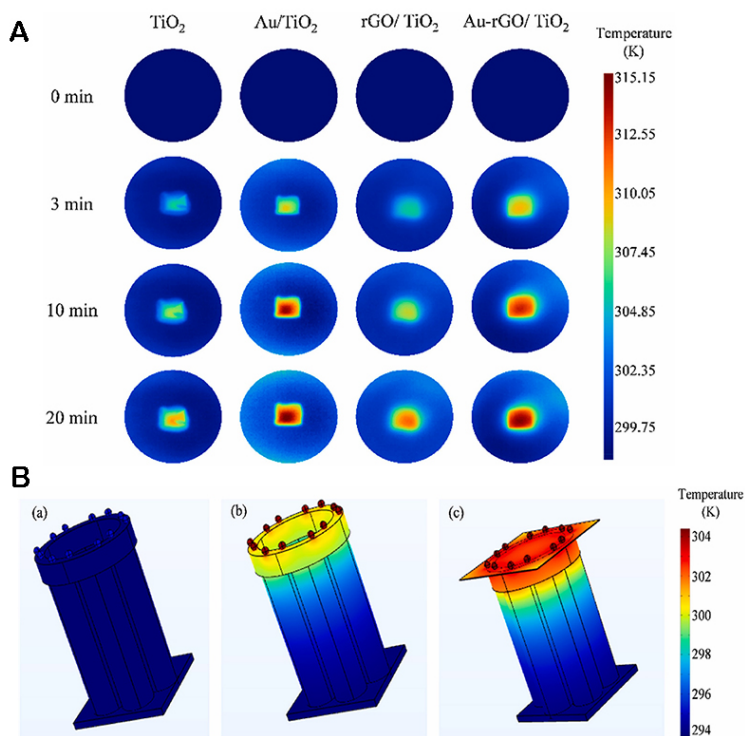


Figure 15. (A) Thermal imaging of TiO₂-based photoelectrodes under AM 1.5 irradiation change over time. (B) Steady-state temperature simulation of Au NPs as nano-heat sources (COMSOL)^[135]. Copyright 2023, Elsevier Ltd.

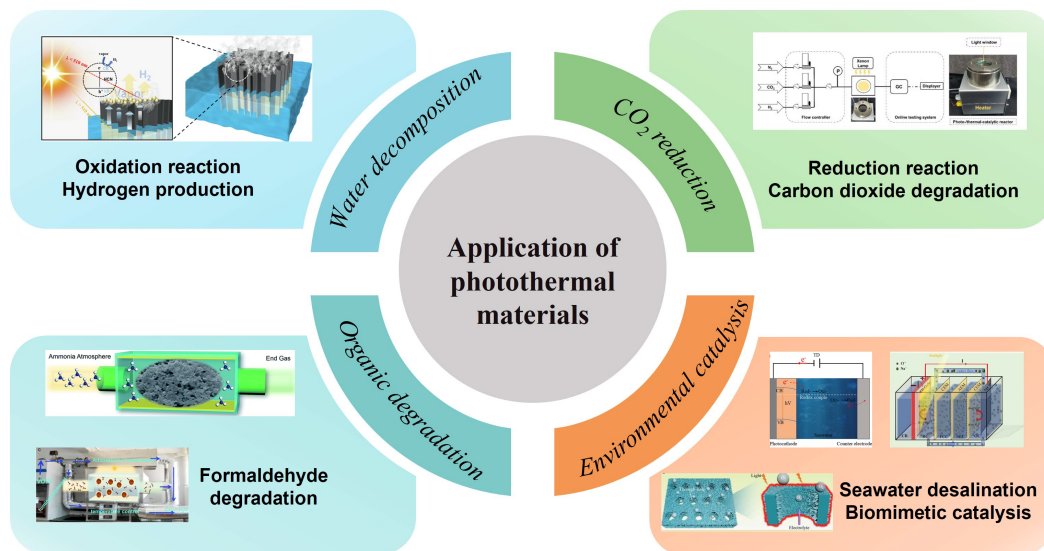


Figure 16. Application direction of photothermal materials.

effectively improve the catalytic performance. For photocatalytic water decomposition, the thermal energy converted by the full spectrum of sunlight can effectively improve the catalytic performance. Table 2 lists the hydrogen production performance of TiO₂ supported by different photothermal materials at elevated temperatures.

Table 2. Hydrogen production rate of photothermal catalytic hydrogen evolution material under thermal effect

Photoanodes	Temperature (°C)	H ₂ evolution rate (mol g ⁻¹ h ⁻¹)	Reference
Ni ₂ P/TiO ₂	90	6,600	[139]
rGO/TiO ₂	70	7,820	[140]
Cu/TiO ₂	90	8,120	[114]
SiO ₂ /Ag@TiO ₂	100	13,300	[141]
Cu ₂ O-rGO/TiO ₂	90	17,800	[142]

Hu *et al.* prepared rGO-modified Cu₂O-supported TiO₂ photocatalysts and applied them to photothermal synergistic catalytic hydrogen production^[142]. Under the condition of PC, the hydrogen production rate reached 178 μmol·h⁻¹ at 90 °C, which is about 4.7 times the sum of photocatalytic and thermocatalytic hydrogen evolution activities (38 μmol·h⁻¹) at 25 °C. It can be seen that the amount of hydrogen evolution under photothermal coupling catalysis is much higher than that under PC or thermocatalysis. According to the analysis of solar spectral light absorption, TiO₂, Cu₂O, and rGO in the composite material represent the utilization of UV light, visible light, and infrared light, respectively, achieving gradient utilization. The photothermal effect produced by graphene between semiconductors can accelerate the rate of electron and hole transfer on the catalyst surface.

Zhang *et al.* also use the gradient absorption of solar energy to co-modify In₂O₃ with transition metals Fe and Cu^[143]. Fe doping widens the radiation response range of the intrinsic part of the semiconductor, while Cu doping is beneficial to the absorption of visible infrared light and produces photothermal synergies. As shown in Figure 17A, the photo-driven photothermal catalytic reaction system (PDS) is built with quartz, and the system energy uses full-spectrum xenon lamps. The catalyst film was placed on the quartz scaffold, and the reaction temperature was maintained by the thermal effect generated by the light catalyst film. The DFT calculation of the reaction process is also carried out, and the results show that the increase of temperature can directly affect the chemical reaction by reducing the energy barrier of RDS.

Ding *et al.* coated CIZS@Ru photocatalysts on the surface of a C-MF net^[144]. In the photocatalyst, C-MF absorbs vision-infrared light, while the photocatalyst captures UV-visible light. A spatially separated photothermal coupling photocatalytic reaction system was designed. The whole device can float on the water surface, reducing the refraction loss of light through the water and the transmission resistance of hydrogen [Figure 17B and C]. The distribution of the photocatalyst on the surface of the photothermal material reduces the local heating distance and helps to improve the influence of local heat on the photocatalytic activity. Driven by the photothermal effect, the hydrogen evolution performance of the material reached 603 mmol h⁻¹ m⁻².

Photocatalysis and water vapor

For the water decomposition process, the increase in temperature will promote the conversion of water into water vapor, increasing the catalytic contact surface.

Han *et al.* prepare the g-C₃N₄ (CW-HCN) system by growing spherical g-C₃N₄ (HCN) on carbonized wood (CW) by hydrothermal methods^[145]. The H₂ precipitation rate reached 2,700.18 μmol m⁻² h⁻¹ under sunlight. As shown in Figure 18A, CW acts as the growth base for the g-C₃N₄ photocatalyst and also acts as a steam generator. The carbonization layer uses visible and near-infrared light in the solar spectrum to produce steam, while the UV light and part of the visible light are absorbed by g-C₃N₄ to produce electron-hole pairs for the decomposition of water. The combination of photoheat and PC greatly expands the utilization of solar photons.

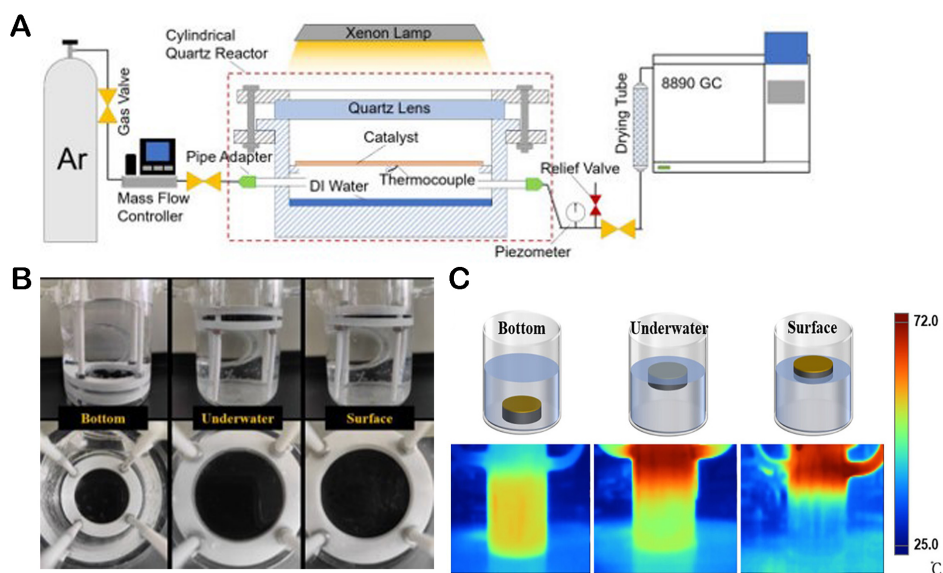


Figure 17. (A) Schematic diagram of a photo-driven photothermal catalytic reaction system (PDS)^[143]. Copyright 2023, American Chemical Society. (B) Physical images of C-MF at different locations in solution. (C) Schematic diagram and thermographic image of C-MF/CIZS@Ru in solution illuminated at different positions for 1 h^[144]. Copyright 2022, American Chemical Society.

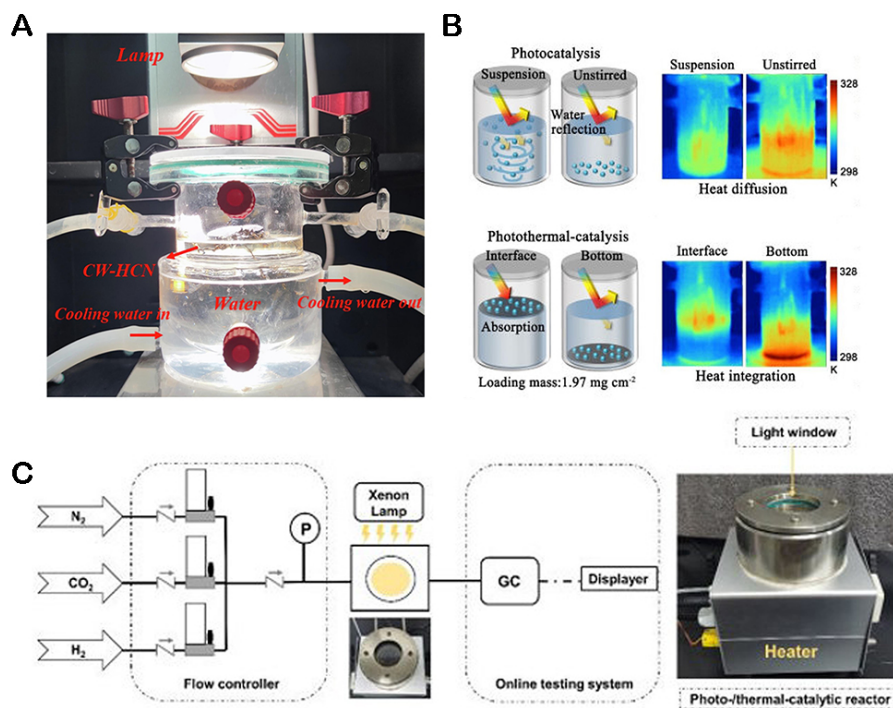


Figure 18. (A) Photo of the photothermal-photocatalytic H₂ evolution system^[145]. Copyright 2023, Academic Press Inc Elsevier Sci. (B) The Schematic of the utilization of sunlight and water splitting performance in liquid-solid and gas-solid systems with different catalyst dispersion states under high light intensity^[146]. Copyright 2023, John Wiley & Sons, Inc. (C) Schematic diagram of a thermocouple-controlled photocatalytic CO₂ reduction device^[147]. Copyright 2021, American Chemical Society.

Li *et al.* design K-SrTiO₃ catalysts loaded with TiN silica wool at the water-air interface^[146]. The thermal effect is used to convert liquid water into water vapor, thereby reducing the reaction-free energy of the

catalyst and improving the permeability of the catalytic product. The photothermal catalytic hydrogen production efficiency can reach $275.46 \text{ mmol m}^{-2} \text{ h}^{-1}$, which is more than twice the decomposition efficiency of liquid water [Figure 18B].

Photothermal catalysis and CO₂ reduction

Photothermal catalysis is used to reduce CO₂ and convert CO₂ into fuel through photothermal catalysis. Wu *et al.* load Nb₂C and Ti₃C₂ onto Ni NPs^[147]. Nb₂C and Ti₃C₂ are two typical MXene materials with photothermal effects, which can improve the photothermal catalytic activity of Ni NPs. In the catalytic reduction process, the temperature of the reaction system was increased by adding strong light. The activity of Nb₂C/Ni was increased with the increase of light intensity, and the CO₂ conversion rate of Nb₂C/Ni NPs reached $8.50 \text{ mol} \cdot \text{g}_{\text{Ni}}^{-1} \cdot \text{h}^{-1}$. In order to explore the effect of its thermal effect on temperature, a reactor was built, as shown in Figure 18C. The temperature of the reactor was controlled by a self-made heating device, and the thermocouple was placed under the catalyst film to explore the CO₂ conversion rate through temperature control.

Photothermal catalysis and organic degradation

PC is a common method used in organic matter degradation, and the efficiency of photocatalytic pollution degradation can be further improved by using the photothermal effect^[148,149]. Huang *et al.* introduced oxygen vacancies into BiOI nanosheets (named BiOI-8) with low concentration nitric acids and applied them to photocatalytic degradation of formaldehyde^[150]. As shown in Figure 19A, the photocatalytic performance of BiOI-8 nanosheets improved with the increase of temperature. The catalytic activity of BiOI-8 nanosheets at 60 °C was 20% higher than that at room temperature. The BiOI-8 nanosheets were tested in an industrial-grade photocatalytic unit [Figure 19B]. Huang *et al.* prepared CeO₂/CeN photocatalysts^[151]. The prepared CeO₂/CeN composites showed higher photothermal catalytic performance than the original CeO₂ in removing organic pollutants. The enhancement of photothermal catalytic activity is due to the formation of the phase interface boundary of effective photothermal catalytic degradation due to the introduction of CeN [Figure 19C and D].

PEC and photothermal effect

PEC and photothermal effect

In the application of photothermal materials in PEC water decomposition, there are more reports on the enhancement of photothermal effects by applying infrared radiation. As shown in Table 3, the photocurrent density of PEC of different materials is significantly improved with its addition.

Xiong *et al.* built CoCr₂O₄/g-C₃N₄ and used the strong absorption of CoCr₂O₄ NPs in the near-infrared region to improve the temperature of the reaction center to improve the performance of PEC^[152]. The simple CoCr₂O₄ NPs did not show photocatalytic activity of PEC hydrogen production, but the average hydrogen production rate under UV-vis-IR was as high as $1,525.1 \text{ } \mu\text{mol g}^{-1} \text{ h}^{-1}$, which was four times higher than that of pure g-C₃N₄.

Lin *et al.* load NCO nanomedles with nickel foam (NF) to promote their OER properties through infrared thermal effects^[153]. The local thermal effect of infrared radiation on the catalyst increases the surface temperature of NCO, which proves that the decrease of electrochemical activation energy caused by infrared thermal effects is the reason for the increase of OER activity. It can be seen from the linear sweep volt (LSV) curve [Figure 20A] that NF/NCO exhibits significantly enhanced OER activity under continuous infrared irradiation. After infrared irradiation, the surface temperature of NF/NCO rose sharply and reached 48.1 °C within 15 s. The nanoneedle arrays of NCO further improve infrared absorption by

Table 3. Compare the performance of PEC with or without NIR

Photoanode	Photothermal effector materials	Photocurrent density (1.23 V _{RHE})	Photocurrent density with NIR (1.23 V _{RHE})	Reference
Au/Ni/ITO/BiVO ₄ @CoPi	Ni	3.28 mA cm ⁻²	5.19 mA cm ⁻²	[83]
NiOOH/FeOOH/Co ₃ O ₄ /BiVO ₄	Co ₃ O ₄	4.49 mA cm ⁻²	6.34 mA cm ⁻²	[88]
Bi ₂ S ₃ /WO ₃	Bi ₂ S ₃	3.60 mA cm ⁻²	4.60 mA cm ⁻²	[96]
PANI/BiVO ₄	PANI	3.01 mA cm ⁻²	4.05 mA cm ⁻²	[118]
CIS/Ni-PPy	PPy	3.75 mA cm ⁻²	6.07 mA cm ⁻²	[119]
Co-Pi/CQDs/Fe ₂ O ₃ /TiO ₂	CQDs	1.65 mA cm ⁻²	3.00 mA cm ⁻²	[124]

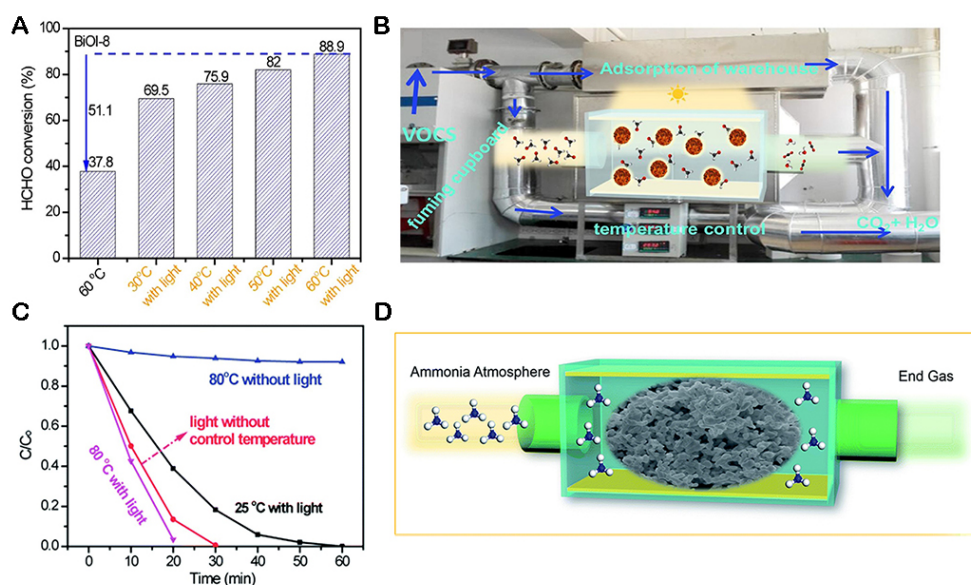


Figure 19. (A) Photocatalytic degradation of HCHO at different temperatures at 45 min. (B) Photograph of large-scale photocatalytic devices^[150]. Copyright 2018, Elsevier Inc. (C) Photo-thermocatalytic performance of pollutant degradation. (D) Representation of the formation of CeO₂/CeN nanorods^[151]. Copyright 2018, Royal Society of Chemistry.

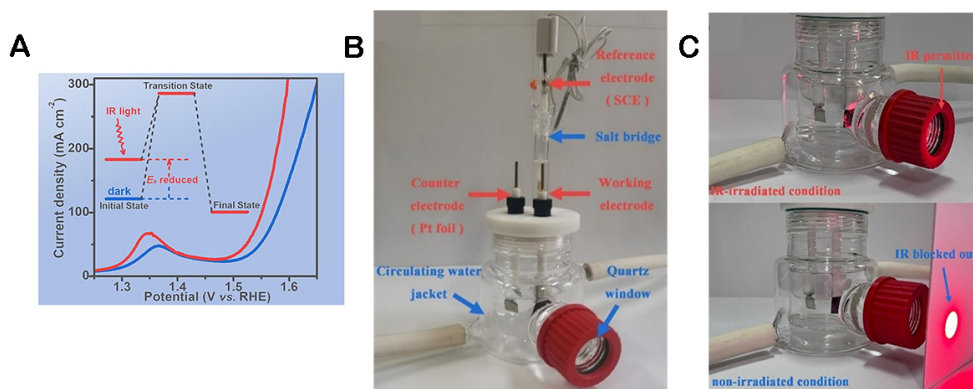


Figure 20. (A) LSV curves obtained on the NF/NiCo₂O₄. (B) Structure of jacketed glass electrochemical cell for PEC performance measurement. (C) NiCo₂O₄ (NF/NiCo₂O₄) electrodes supported by nickel foam with and without NIR^[153]. Copyright 2023, Academic Press Inc Elsevier Sci.

providing a larger specific surface area and reduced infrared diffuse reflection. The reaction devices are shown in [Figure 20B](#) and [C](#).

Dong *et al.* design a co-modified N,Ni-BVO/N-TNA photoanode with N and Ni double-point defects on the basis of $\text{BiVO}_4/\text{TiO}_2$ heterojunction photocatalysts^[154]. Through co-doping, oxygen vacancies are formed, greatly improving the photothermal effect of the infrared drive, which makes the maximum temperature of the lifting solution rise to 48.6 °C. The increase of solution temperature also decreases the interfacial resistance of the heterojunction, leading to faster electron transport.

Thermal effect of PEC combined with perovskite batteries

Perovskite is one of the most widely used materials in solar cells. PEC can be realized by its effect of light absorption and light heat transfer^[155].

Tang *et al.* design a composite photoelectrode ($\text{Au/Ni/ITO/BiVO}_4\text{@CoPi}$) with both photothermal and photoelectric conversion^[83]. As shown in [Figure 21A](#), bismuth vanadate and perovskite cells absorb sunlight in the bands of 300-505 nm and 505-850 nm to generate sufficient water decomposition photovoltage and photocurrent. The 850-2,000 nm (infrared light region) nanometer metal nickel layer is used to generate heat to promote the photogenic charge collection process and water decomposition reaction rate of the electrode. The system can increase the electrolyte temperature from 293.15 K to 328.15 K by self-drive and achieve 4.28 mA cm⁻² light-driven water and light decomposition current. The photothermal substrate (Au/Ni/ITO) was tested by an infrared imager at a temperature of 62.0 °C under infrared irradiation for only 8 min, which verified the significant photothermal conversion effect of the material.

Wang *et al.* deposit NiFe layer double hydroxide (NiFe LDH) on a three-dimensional CNT scaffold^[129]. A water decomposition system was constructed by connecting a CNTs@NiFe LDH//Pt/C electrochemical cell (EC) with a semitransparent perovskite solar cell (ST-PSC) micromodule in series [[Figure 21B](#)]. Infrared radiation can pass through the translucent PSCs, introducing a photothermal effect on the EC electrode, thus making better use of the full solar spectrum. With the aid of the photothermal effect, the STH efficiency of the tandem system is improved by 12%. The reaction device is shown in [Figure 21C](#).

Photothermal effect of PEC and seawater desalination

In the earth's water resources, the effective use of seawater can effectively achieve environmental energy saving and water resource regeneration^[156].

Cai *et al.* use the photovoltaic and photothermal coupling effects of GeSe-based photoelectrodes to be applied in solar desalination^[157]. When combined under the irradiation of AM 1.5 G, it was found that the temperature of the GeSe system was significantly higher than that of the solution (up to 323 K) because GeSe converted part of the absorbed visible light into heat. Therefore, thermoelectric devices (TD) with GeSe bases can be introduced to make full use of the full spectrum of solar energy. As shown in [Figure 21D](#), the TD-GeSe-based solar desalination battery is integrated and coupled with the GeSe-based photocathode to form a TD-GeSe-based solar desalination battery and placed between the desalination chamber and the cooling chamber to achieve sustainable and efficient seawater desalination. This method effectively converts natural seawater to seawater close to fresh water, reducing the total dissolved solid solution and salinity of the original solution from 29 g L⁻¹ and 27 ppm to about 1.0 g L⁻¹ and 0.7 ppm, respectively.

Photothermal effect and bionic structure of PEC

The research of PEC is nothing more than an artificial way to achieve biological photosynthesis, and the

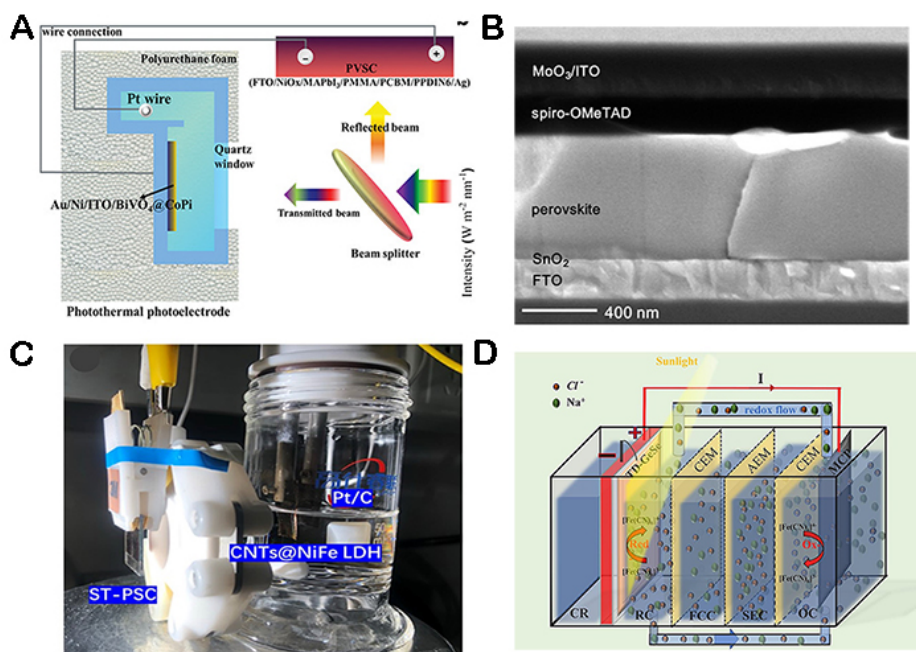


Figure 21. (A) L-type photothermal PEC-PV device schematic^[83]. Copyright 2022, John Wiley & Sons, Inc. (B) Cross-section SEM image of the semitransparent PSC. (C) The integrated ST-PSC+EC system for water splitting^[129]. Copyright 2023, Elsevier Sci. (D) Structure and schematic diagram of the solar desalination system^[157]. Copyright 2023, Elsevier Sci.

construction of biomimetic structure materials applied to PEC can effectively improve its photoelectric catalytic and photothermal catalytic performance^[158].

Inspired by the photosynthesis of plant leaves, Zhou *et al.* load the photothermal $\text{MoS}_2/\text{FeCoNiS}$ nanotubes onto porous NF (PNF)^[159]. As shown in Figure 22A, PNF and $\text{MoS}_2/\text{FeCoNiS}$ resemble the structure and epidermis of leaf tissue, respectively. The stomatal structure of PNF promotes bubble transport in OER, while $\text{MoS}_2/\text{FeCoNiS}$ increases light absorption and photothermal conversion. As the electrolyte temperature increases from 25 °C to 55 °C, the OER performance of $\text{MoS}_2/\text{FeCoNiS-NT@PNF}$ improves significantly. With the help of bionic structures and photothermal effect, the $\text{MoS}_2/\text{FeCoNiS-NT@PNF}$ electrode achieves a current density of 50 mA cm⁻² at 1.44 V (*vs.* RHE).

Zhang *et al.* prepare a $\text{MoS}_2/\text{Ni}_3\text{S}_2$ -coated carbon nanowires (CA) composite ($\text{MoS}_2/\text{Ni}_3\text{S}_2@\text{CA}$) by tracking the sun to raise the temperature from a natural sunflower head^[160]. $\text{MoS}_2/\text{Ni}_3\text{S}_2@\text{CA}$ has a honeycomb structure similar to the microstructure of sunflower petals. The carbon nanowire substrate with three-dimensional multistage pore structures can increase the active sites of catalyst nanosheets and accelerate the transfer process of bubbles and electrolytes. The biomimetic sunflower micro-nanostructures are able to better capture sunlight and efficiently and quickly convert light into heat. The current density of $\text{MoS}_2/\text{Ni}_3\text{S}_2@\text{CA}$ is 10 mA cm⁻² at 1.51 V [Figure 22B].

CONCLUSIONS

In this paper, the basic principle of the photothermal effect is briefly introduced, and several kinds of photothermal materials widely reported at present are reviewed. The reason why the photothermal effect improves the photocatalytic performance is analyzed from the perspective of physical models and principle analysis. The introduction of thermal effects can improve the thermodynamic and kinetic effects of the

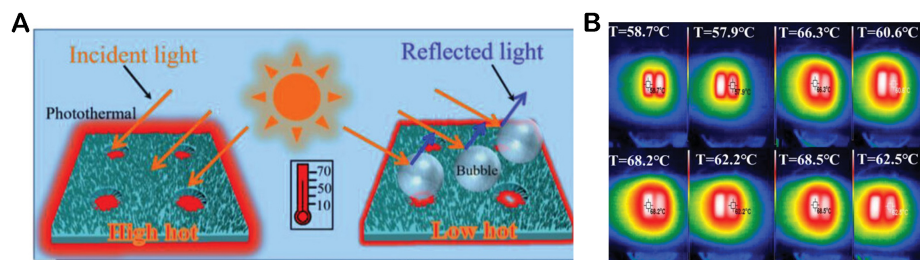


Figure 22. (A) Photothermal conversion and reflection of incident photons ($h\nu$) at electrolyte/bubble interface^[159]. Copyright 2023, John Wiley & Sons, Inc. (B) Thermal images of $\text{Ni}_3\text{S}_2/\text{MoS}_2/\text{CC}$ at different constant temperatures^[160]. Copyright 2023, John Wiley & Sons, Inc.

catalytic reaction itself. At the same time, most photothermal materials themselves produce more excitons due to the increase of temperature. The characteristics of different types of photothermal materials are reviewed, and their respective advantages are analyzed. Finally, the application of photothermal effects in PC and PEC in reduction, oxidation, and other specific fields is summarized. Whether it is photothermal catalysis or photothermoelectric catalysis, it is an innovation of traditional photocatalytic technology. The addition of thermal effects is not a simple one-plus-one process but rather a coordination of the two effects from the mechanism to achieve improvement. From the perspective of long-term development, it is a feasible industrial practice to improve energy utilization and reduce losses through a variety of energy cooperative coupling.

Although the development of PC/PEC photothermal materials is expected in the future, there are still some challenges:

1. Photothermal catalysts: currently, precious metal-supported photothermal catalysts are the most widely used in current research because of their high catalytic activity. However, their high cost limits their application and promotion. In addition, challenges related to poor light absorption and conversion ability, low activity, and low stability of photothermal materials persist as fundamental issues in the research and development of photothermal materials. In summary, the development of low-cost and high-activity materials is the main direction of further research.
2. Combination of photothermal materials and photocatalytic materials: in the current reports on the application of photothermal materials to PC, most of the photothermal materials and photocatalysts are composites with a layered structure. The way of their mutual connection and action is generally through physical connection or hydrogen bond connection, and the combination degree of the two needs to be further improved. If photothermal and photocatalytic materials can be combined at the nanoscale, it will help to improve the energy and electron conduction between these materials so as to achieve higher conversion efficiency.
3. Photothermal reactor: the current photothermal reaction system will build more devices through external connections to achieve higher conversion efficiency. However, this approach seems to go against the original intention of PC itself to achieve energy conversion in a clean and efficient way. Therefore, for future photothermal reactors, it is recommended to utilize sunlight as the only light source and harness its energy to achieve catalytic effects.

4. Development of the photothermal materials industry: many factors influence the performance of photothermal catalysis at present, and its effectiveness is determined by different conditions, such as light intensity, light band, bias pressure, and reactor temperature. However, the current research field has yet to establish a standardized evaluation system for this series of photocatalysts, hindering the development of an industrial evaluation framework. In addition, the monitoring and control of various parameters of the reaction process have not been able to determine clear process parameters. There is still a long way to go for the large-scale industrial promotion of photothermal materials.

DECLARATIONS

Authors' contributions

Characterizing and writing the original draft: Zhang J

Review and supervision: Ye KH, Shi J

Editing the manuscript: Tang T, Yang R, Wang G

Availability of data and materials

Not applicable.

Financial support and sponsorship

None.

Conflicts of interest

All authors declared that there are no conflicts of interest.

Ethical approval and consent to participate

Not applicable.

Consent for publication

Not applicable.

Copyright

© The Author(s) 2024.

REFERENCES

1. Fares RL, Webber ME. The impacts of storing solar energy in the home to reduce reliance on the utility. *Nat Energy* 2017;2:17001. DOI
2. Kammen DM, Sunter DA. City-integrated renewable energy for urban sustainability. *Science* 2016;352:922-8. DOI PubMed
3. Lelieveld J, Evans JS, Fnais M, Giannadaki D, Pozzer A. The contribution of outdoor air pollution sources to premature mortality on a global scale. *Nature* 2015;525:367-71. DOI PubMed
4. Dawood F, Anda M, Shafiullah G. Hydrogen production for energy: an overview. *Int J Hydrog Energy* 2020;45:3847-69. DOI
5. Tee SY, Win KY, Teo WS, et al. Recent progress in energy-driven water splitting. *Adv Sci* 2017;4:1600337. DOI PubMed PMC
6. Zou X, Zhang Y. Noble metal-free hydrogen evolution catalysts for water splitting. *Chem Soc Rev* 2015;44:5148-80. DOI PubMed
7. Muradov N. Low to near-zero CO₂ production of hydrogen from fossil fuels: status and perspectives. *Int J Hydrog Energy* 2017;42:14058-88. DOI
8. Ran J, Jaroniec M, Qiao SZ. Cocatalysts in semiconductor-based photocatalytic CO₂ reduction: achievements, challenges, and opportunities. *Adv Mater* 2018;30:1704649. DOI PubMed
9. Abbott D. Keeping the energy debate clean: how do we supply the world's energy needs? *Proc IEEE* 2010;98:42-66. DOI
10. Thalluri SM, Bai L, Lv C, Huang Z, Hu X, Liu L. Strategies for semiconductor/electrocatalyst coupling toward solar-driven water splitting. *Adv Sci* 2020;7:1902102. DOI PubMed PMC
11. Fujishima A, Honda K. Electrochemical photolysis of water at a semiconductor electrode. *Nature* 1972;238:37-8. DOI
12. Butburee T, Bai Y, Wang H, et al. 2D Porous TiO₂ single-crystalline nanostructure demonstrating high photo-electrochemical water splitting performance. *Adv Mater* 2018;30:e1705666. DOI

13. Liu X, Wang F, Wang Q. Nanostructure-based WO₃ photoanodes for photoelectrochemical water splitting. *Phys Chem Chem Phys* 2012;14:7894-911. DOI
14. Chen D, Xie Z, Tong Y, Huang Y. Review on BiVO₄-based photoanodes for photoelectrochemical water oxidation: the main influencing factors. *Energy Fuels* 2022;36:9932-49. DOI
15. Hsu YK, Chen YC, Lin YG. Novel ZnO/Fe₂O₃ core-shell nanowires for photoelectrochemical water splitting. *ACS Appl Mater Interfaces* 2015;7:14157-62. DOI PubMed
16. Zhang Y, Pan D, Tao Y, et al. Photoelectrocatalytic reduction of CO₂ to syngas via SnOx-enhanced Cu₂O nanowires photocathodes. *Adv Funct Materials* 2022;32:2109600. DOI
17. Pan L, Muhammad T, Ma L, et al. MOF-derived C-doped ZnO prepared via a two-step calcination for efficient photocatalysis. *Appl Catal B* 2016;189:181-91. DOI
18. Wang L, Shi X, Jia Y, Cheng H, Wang L, Wang Q. Recent advances in bismuth vanadate-based photocatalysts for photoelectrochemical water splitting. *Chin Chem Lett* 2021;32:1869-78. DOI
19. Zhang J, Huang Y, Lu X, Yang J, Tong Y. Enhanced BiVO₄ photoanode photoelectrochemical performance via borate treatment and a NiFeOx cocatalyst. *ACS Sustain Chem Eng* 2021;9:8306-14. DOI
20. Lin F, Boettcher SW. Adaptive semiconductor/electrocatalyst junctions in water-splitting photoanodes. *Nat Mater* 2014;13:81-6. DOI PubMed
21. Xie Z, Chen D, Zhai J, Huang Y, Ji H. Charge separation via synergy of homojunction and electrocatalyst in BiVO₄ for photoelectrochemical water splitting. *Appl Catal B* 2023;334:122865. DOI
22. Digdaya IA, Adhyaksa GWP, Trześniewski BJ, Garnett EC, Smith WA. Interfacial engineering of metal-insulator-semiconductor junctions for efficient and stable photoelectrochemical water oxidation. *Nat Commun* 2017;8:15968. DOI PubMed PMC
23. Bae D, Seger B, Vesborg PC, Hansen O, Chorkendorff I. Strategies for stable water splitting via protected photoelectrodes. *Chem Soc Rev* 2017;46:1933-54. DOI PubMed
24. Chen D, Liu Z, Guo Z, Yan W, Ruan M. Decorating Cu₂O photocathode with noble-metal-free Al and NiS cocatalysts for efficient photoelectrochemical water splitting by light harvesting management and charge separation design. *Chem Eng J* 2020;381:122655. DOI
25. Zandi O, Hamann TW. Enhanced water splitting efficiency through selective surface state removal. *J Phys Chem Lett* 2014;5:1522-6. DOI PubMed
26. Sivula K. Metal oxide photoelectrodes for solar fuel production, surface traps, and catalysis. *J Phys Chem Lett* 2013;4:1624-33. DOI PubMed
27. Liu W, Liu H, Dang L, et al. Amorphous Cobalt-iron hydroxide nanosheet electrocatalyst for efficient electrochemical and photoelectrochemical oxygen evolution. *Adv Funct Mater* 2017;27:1603904. DOI
28. Meng Q, Zhang B, Yang H, et al. Remarkable synergy of borate and interfacial hole transporter on BiVO₄ photoanodes for photoelectrochemical water oxidation. *Mater Adv* 2021;2:4323-32. DOI
29. Liang Z, Li M, Ye K, et al. Systematic engineering of BiVO₄ photoanode for efficient photoelectrochemical water oxidation. *Carbon Energy* 2023:e413. DOI
30. Yang J, Zhou J, Huang Y, Tong Y. Lanthanide-based dual modulation in hematite nanospindles for enhancing the photocatalytic performance. *ACS Appl Nano Mater* 2022;5:8557-65. DOI
31. Ye K, Hu P, Liu K, et al. New findings for the much-promised hematite photoanodes with gradient doping and overlayer elaboration. *Solar RRL* 2022;6:2270061. DOI
32. Liu J, Chen W, Sun Q, et al. Oxygen vacancies enhanced WO₃/BiVO₄ photoanodes modified by cobalt phosphate for efficient photoelectrochemical water splitting. *ACS Appl Energy Mater* 2021;4:2864-72. DOI
33. Yang W, Prabhakar RR, Tan J, Tilley SD, Moon J. Strategies for enhancing the photocurrent, photovoltage, and stability of photoelectrodes for photoelectrochemical water splitting. *Chem Soc Rev* 2019;48:4979-5015. DOI PubMed
34. Wang S, Chen P, Bai Y, Yun JH, Liu G, Wang L. New BiVO₄ dual photoanodes with enriched oxygen vacancies for efficient solar-driven water splitting. *Adv Mater* 2018;30:e1800486. DOI
35. Butson JD, Sharma A, Tournet J, et al. Unlocking ultra-high performance in immersed solar water splitting with optimised energetics. *Adv Energy Mater* 2023;13:2301793. DOI
36. Kim H, Seo JW, Chung W, et al. Thermal effect on photoelectrochemical water splitting toward highly solar to hydrogen efficiency. *ChemSusChem* 2023;16:e202202017. DOI
37. Li T, Zou Y, Liu Z. Magnetic-thermal external field activate the pyro-magnetic effect of pyroelectric crystal (NaNbO₃) to build a promising multi-field coupling-assisted photoelectrochemical water splitting system. *Appl Catal B* 2023;328:122486. DOI
38. Khan H, Lone IH, Lofland SE, Ramanujachary KV, Ahmad T. Exploiting multiferroicity of TbFeO₃ nanoparticles for hydrogen generation through photo/electro/photoelectro-catalytic water splitting. *Int J Hydrogen Energy* 2023;48:5493-505. DOI
39. Han Q, Han Z, Wang Y, et al. Enhanced photocatalytic hydrogen evolution by piezoelectric effects based on MoSe₂/Se-decorated CdS nanowire edge-on heterostructure. *J Colloid Interface Sci* 2023;630:460-72. DOI
40. Kai J, Saito R, Terabaru K, Li H, Nakajima H, Ito K. Effect of temperature on the performance of polymer electrolyte membrane water electrolysis: numerical analysis of electrolysis voltage considering gas/liquid two-phase flow. *J Electrochem Soc* 2019;166:F246. DOI
41. Barco-burgos J, Eicker U, Saldaña-robles N, Saldaña-robles A, Alcántar-camarena V. Thermal characterization of an alkaline

- electrolysis cell for hydrogen production at atmospheric pressure. *Fuel* 2020;276:117910. DOI
42. Tang S, Xing X, Yu W, et al. Synergizing photo-thermal H₂ and photovoltaics into a concentrated sunlight use. *iScience* 2020;23:101012. DOI PubMed PMC
43. Mateo D, Cerrillo JL, Durini S, Gascon J. Fundamentals and applications of photo-thermal catalysis. *Chem Soc Rev* 2021;50:2173-210. DOI
44. Yu F, Wang C, Li Y, et al. Enhanced solar photothermal catalysis over solution plasma activated TiO₂. *Adv Sci* 2020;7:2000204. DOI
45. Ghossoub M, Xia M, Duchesne PN, Segal D, Ozin G. Principles of photothermal gas-phase heterogeneous CO₂ catalysis. *Energy Environ Sci* 2019;12:1122-42. DOI
46. Xiao JD, Jiang HL. Metal-organic frameworks for photocatalysis and photothermal catalysis. *Acc Chem Res* 2019;52:356-66. DOI PubMed
47. Niu F, Wang D, Li F, Liu Y, Shen S, Meyer TJ. Hybrid photoelectrochemical water splitting systems: from interface design to system assembly. *Adv Energy Mater* 2020;10:1900399. DOI
48. Tayebi M, Lee B. Recent advances in BiVO₄ semiconductor materials for hydrogen production using photoelectrochemical water splitting. *Renew Sustain Energy Rev* 2019;111:332-43. DOI
49. Maeda K, Domen K. Photocatalytic water splitting: recent progress and future challenges. *J Phys Chem Lett* 2010;1:2655-61. DOI
50. Sang Y, Zhao Z, Zhao M, Hao P, Leng Y, Liu H. From UV to near-infrared, WS₂ nanosheet: a novel photocatalyst for full solar light spectrum photodegradation. *Adv Mater* 2015;27:363-9. DOI
51. Zhang J, Chen H, Duan X, Sun H, Wang S. Photothermal catalysis: from fundamentals to practical applications. *Mater Today* 2023;68:234-53. DOI
52. Wang X, Ma S, Liu B, Wang S, Huang W. Imperfect makes perfect: defect engineering of photoelectrodes towards efficient photoelectrochemical water splitting. *Chem Commun* 2023;59:10044-66. DOI
53. Wang Y, Zhang J, Balogun M, Tong Y, Huang Y. Oxygen vacancy-based metal oxides photoanodes in photoelectrochemical water splitting. *Mater Today Sustain* 2022;18:100118. DOI
54. Zhao L, Liu Y, Xing R, Yan X. Supramolecular photothermal effects: a promising mechanism for efficient thermal conversion. *Angew Chem Int Ed* 2020;59:3793-801. DOI
55. Seh ZW, Kibsgaard J, Dickens CF, Chorkendorff I, Nørskov JK, Jaramillo TF. Combining theory and experiment in electrocatalysis: insights into materials design. *Science* 2017;355:eaad4998. DOI PubMed
56. Kim JH, Lee JS. Elaborately modified BiVO₄ photoanodes for solar water splitting. *Adv Mater* 2019;31:e1806938. DOI PubMed
57. Li Z, Luo W, Zhang M, Feng J, Zou Z. Photoelectrochemical cells for solar hydrogen production: current state of promising photoelectrodes, methods to improve their properties, and outlook. *Energy Environ Sci* 2013;6:347-70. DOI
58. Stepanov IA. The heats of chemical reactions: the Van't-Hoff equation and calorimetry. *Z Phy Chem* 2005;219:1089-97. DOI
59. Kweon KE, Hwang GS. Structural phase-dependent hole localization and transport in bismuth vanadate. *Phys Rev B* 2013;87:205202. DOI
60. Tan HL, Amal R, Ng YH. Alternative strategies in improving the photocatalytic and photoelectrochemical activities of visible light-driven BiVO₄: a review. *J Mater Chem A* 2017;5:16498-521. DOI
61. Matthies M, Beulke S. Considerations of temperature in the context of the persistence classification in the EU. *Environ Sci Eur* 2017;29:15. DOI PubMed PMC
62. Pendlebury SR, Barroso M, Cowan AJ, et al. Dynamics of photogenerated holes in nanocrystalline α -Fe₂O₃ electrodes for water oxidation probed by transient absorption spectroscopy. *Chem Commun* 2011;47:716-8. DOI
63. Cowan AJ, Barnett CJ, Pendlebury SR, et al. Activation energies for the rate-limiting step in water photooxidation by nanostructured α -Fe₂O₃ and TiO₂. *J Am Chem Soc* 2011;133:10134-40. DOI
64. Sleutels TH, Darus L, Hamelers HV, Buisman CJ. Effect of operational parameters on coulombic efficiency in bioelectrochemical systems. *Bioresour Technol* 2011;102:11172-6. DOI PubMed
65. Harmon M, Gamba IM, Ren K. Numerical algorithms based on Galerkin methods for the modeling of reactive interfaces in photoelectrochemical (PEC) solar cells. *J Comput Phys* 2016;327:140-67. DOI
66. Kreider ME, Gallo A, Back S, et al. Precious metal-free nickel nitride catalyst for the oxygen reduction reaction. *ACS Appl Mater Interfaces* 2019;11:26863-71. DOI
67. Liu C, Wang Z, Zhang T, Zhang Y, Su J. Photo/thermal dual-activation improves the photocurrent of bismuth vanadate for pec water splitting. *ChemElectroChem* 2022;9:e202200646. DOI
68. Ye X. Elevated temperature photo-electrochemical water splitting. 2016. Available from: <http://purl.stanford.edu/vy785kk1866> [Last accessed on 30 Nov 2023]
69. Isik M, Delice S, Gasanly N. Temperature-dependent optical properties of TiO₂ nanoparticles: a study of band gap evolution. *Opt Quant Electron* 2023;55:905. DOI
70. Landman A, Dotan H, Shter GE, et al. Photoelectrochemical water splitting in separate oxygen and hydrogen cells. *Nat Mater* 2017;6:646-51. DOI
71. Zhao H, Tian F, Wang R, Chen R. A review on bismuth-related nanomaterials for photocatalysis. *Rev Adv Sci Eng* 2014;3:3-27. DOI
72. Varshni YP. Temperature dependence of the elastic constants. *Phys Rev B* 1970;2:3952-8. DOI
73. Leszczynski M, Suski T, Teisseyre H, et al. Thermal expansion of gallium nitride. *J Appl Phys* 1994;76:4909-11. DOI
74. Hsu K, Wang C, Liu C. The growth of GaN nanorods with different temperature by molecular beam epitaxy. *J Electrochem Soc*

- 2010;157:K109. DOI
75. Ye CH, Fang XS, Wang M, Zhang LD. Temperature-dependent photoluminescence from elemental sulfur species on ZnS nanobelts. *J Appl Phys* 2006;99:063504. DOI
 76. Pejova B, Abay B, Bineva I. Temperature dependence of the band-gap energy and sub-band-gap absorption tails in strongly quantized ZnSe nanocrystals deposited as thin films. *J Phys Chem C* 2010;114:15280-91. DOI
 77. Lee MG, Kim DH, Sohn W, et al. Conformally coated BiVO₄ nanodots on porosity-controlled WO₃ nanorods as highly efficient type II heterojunction photoanodes for water oxidation. *Nano Energy* 2016;28:250-60. DOI
 78. Tang R, Yin R, Zhou S, et al. Layered MoS₂ coupled MOFs-derived dual-phase TiO₂ for enhanced photoelectrochemical performance. *J Mater Chem A* 2017;5:4962-71. DOI
 79. Lee SA, Lee TH, Kim C, et al. Tailored NiO_x/Ni cocatalysts on silicon for highly efficient water splitting photoanodes via pulsed electrodeposition. *ACS Catal* 2018;8:7261-9. DOI
 80. Chen D, Li X, Huang J, Chen Y, Liu Z, Huang Y. Boosting charge transfer of Fe doping BiVO₄/CoO_x for photoelectrochemical water splitting. *ACS Appl Energy Mater* 2023;6:8495-502. DOI
 81. Pejova B, Abay B. Nanostructured CdSe films in low size-quantization regime: temperature dependence of the band gap energy and sub-band gap absorption tails. *J Phys Chem C* 2011;115:23241-55. DOI
 82. Zhang L, Ye X, Boloor M, Poletayev A, Melosh NA, Chueh WC. Significantly enhanced photocurrent for water oxidation in monolithic Mo: BiVO₄/SnO₂/Si by thermally increasing the minority carrier diffusion length. *Energy Environ Sci* 2016;9:2044-52. DOI
 83. Tang S, Qiu W, Xu X, et al. Harvesting of infrared part of sunlight to enhance polaron transport and solar water splitting. *Adv Funct Materials* 2022;32:2110284. DOI
 84. Zhou C, Zhang L, Tong X, Liu M. Temperature effect on photoelectrochemical water splitting: a model study based on BiVO₄ photoanodes. *ACS Appl Mater Interfaces* 2021;13:61227-36. DOI
 85. Wang Z, Yang C, Lin T, et al. Visible-light photocatalytic, solar thermal and photoelectrochemical properties of aluminium-reduced black titania. *Energy Environ Sci* 2013;6:3007-14. DOI
 86. Dias P, Lopes T, Andrade L, Mendes A. Temperature effect on water splitting using a Si-doped hematite photoanode. *J Power Sources* 2014;272:567-80. DOI
 87. Ye X, Yang J, Boloor M, Melosh NA, Chueh WC. Thermally-enhanced minority carrier collection in hematite during photoelectrochemical water and sulfite oxidation. *J Mater Chem A* 2015;3:10801-10. DOI
 88. He B, Jia S, Zhao M, et al. General and robust photothermal-heating-enabled high-efficiency photoelectrochemical water splitting. *Adv Mater* 2021;33:2004406. DOI
 89. Zhang Q, Ning X, Fan Y, et al. Insight into interface charge regulation through the change of the electrolyte temperature toward enhancing photoelectrochemical water oxidation. *J Colloid Interface Sci* 2021;588:31-9. DOI
 90. He B, Zhao F, Yi P, et al. Spinel-oxide-integrated BiVO₄ photoanodes with photothermal effect for efficient solar water oxidation. *ACS Appl Mater Interfaces* 2021;13:48901-12. DOI
 91. Huang J, Hu X, Wang J, et al. Unraveling photothermal-enhanced bulk charge transport and surface oxygen reactions in TiO₂ photoanodes for highly efficient photoelectrochemical water oxidation. *Chem Eng J* 2023;462:142246. DOI
 92. Hu X, Huang J, Cao Y, et al. Photothermal-boosted polaron transport in Fe₂O₃ photoanodes for efficient photoelectrochemical water splitting. *Carbon Energy* 2023;5:e369. DOI
 93. Lu X, Ye K, Zhang S, et al. Amorphous type FeOOH modified defective BiVO₄ photoanodes for photoelectrochemical water oxidation. *Chem Eng J* 2022;428:131027. DOI
 94. Zhang Y, Huang Y, Zhu SS, et al. Covalent S-O bonding enables enhanced photoelectrochemical performance of Cu₂S/Fe₂O₃ heterojunction for water splitting. *Small* 2021;17:2100320. DOI
 95. Xue F, Wu H, Liu Y, et al. CuS nanosheet-induced local hot spots on g-C₃N₄ boost photocatalytic hydrogen evolution. *Int J Hydrog Energy* 2023;48:6346-57. DOI
 96. Zhao F, Sheng H, Sun Q, et al. Harvesting the infrared part of solar light to promote charge transfer in Bi₂S₃/WO₃ photoanode for enhanced photoelectrochemical water splitting. *J Colloid Interface Sci* 2022;621:267-74. DOI
 97. Deng C, Peng L, Ling X, et al. Construction of S-scheme Zn_{0.2}Cd_{0.8}S/biochar aerogel architectures for boosting photocatalytic hydrogen production under sunlight irradiation. *J Clean Prod* 2023;414:137616. DOI
 98. Tai Z, Sun G, Zhang X, et al. Embedding laser-generated CdTe nanocrystals into ultrathin ZnIn₂S₄ nanosheets with sulfur vacancies for boosted photocatalytic H₂ evolution. *J Mater Sci Technol* 2023;166:113-22. DOI
 99. Wang K, Liu J, Tao Y, Benetti D, Rosei F, Sun X. Temperature-dependence photoelectrochemical hydrogen generation based on alloyed quantum dots. *J Phys Chem C* 2022;126:174-82. DOI
 100. Li L, Shi H, Yu H, et al. Ultrathin MoSe₂ nanosheet anchored CdS-ZnO functional paper chip as a highly efficient tandem Z-scheme heterojunction photoanode for scalable photoelectrochemical water splitting. *Appl Catal B* 2021;292:120184. DOI
 101. Guo MJ, Zhao TY, Xing ZP, et al. Hollow Octahedral Cu_{2-x}S/CdS/Bi₂S₃ p-n-p type tandem heterojunctions for efficient photothermal effect and robust visible-light-driven photocatalytic performance. *ACS Appl Mater Interfaces* 2020;12:40328-38. DOI
 102. Zhong W, Wang C, Zhao H, et al. Synergistic effect of photo-thermal catalytic glycerol reforming hydrogen production over 2D Au/TiO₂ nanoflakes. *Chem Eng J* 2022;446:137063. DOI
 103. Valenti M, Jonsson MP, Biskos G, Schmidt-ott A, Smith WA. Plasmonic nanoparticle-semiconductor composites for efficient solar

- water splitting. *J Mater Chem A* 2016;4:17891-912. DOI
104. Cushing SK, Li J, Bright J, et al. Controlling plasmon-induced resonance energy transfer and hot electron injection processes in metal@TiO₂ core-shell nanoparticles. *J Phys Chem C* 2015;119:16239-44. DOI
 105. Lee S, Sun Y, Cao Y, Kang SH. Plasmonic nanostructure-based bioimaging and detection techniques at the single-cell level. *Trends Analyt Chem* 2019;117:58-68. DOI
 106. Zhang Z, Zhang L, Hedhili MN, Zhang H, Wang P. Plasmonic gold nanocrystals coupled with photonic crystal seamlessly on TiO₂ nanotube photoelectrodes for efficient visible light photoelectrochemical water splitting. *Nano Lett* 2013;13:14-20. DOI
 107. Liu ZW, Hou WB, Pavaskar P, Aykol M, Cronin SB. Plasmon resonant enhancement of photocatalytic water splitting under visible illumination. *Nano Lett* 2011;11:1111-16. DOI
 108. Tang T, Li M, Liang Z, et al. Promoting plasmonic hot hole extraction and photothermal effect for the oxygen evolution reactions. *Chemistry* 2023;29:e202300225. DOI
 109. Agarwal D, Aspetti CO, Cargnello M, et al. Engineering localized surface plasmon interactions in gold by silicon nanowire for enhanced heating and photocatalysis. *Nano Lett* 2017;17:1839-45. DOI
 110. Huang Y, Long B, Tang M, et al. Bifunctional catalytic material: an ultrastable and high-performance surface defect CeO₂ nanosheets for formaldehyde thermal oxidation and photocatalytic oxidation. *Appl Catal B* 2016;181:779-87. DOI
 111. Subramanyam P, Meena B, Sinha GN, Deepa M, Subrahmanyam C. Decoration of plasmonic Cu nanoparticles on WO₃/Bi₂S₃ QDs heterojunction for enhanced photoelectrochemical water splitting. *Int J Hydrog Energy* 2020;45:7706-15. DOI
 112. Saeed S, Siddique H, Dai R, et al. Enhanced PEC water splitting performance of silver nanoparticle-coated CdS nanowire photoanodes: the role of silver deposition. *J Phys Chem C* 2021;45:7542-51. DOI
 113. Gelija D, Loka C, Goddati M, Bak N, Lee J, Kim MD. Integration of Ag plasmonic metal and WO₃/InGa_N heterostructure for photoelectrochemical water splitting. *Acs Appl Mater Interfaces* 2023;15:34883-94. DOI
 114. Song R, Liu M, Luo B, Geng J, Jing D. Plasmon-induced photothermal effect of sub-10-nm Cu nanoparticles enables boosted full-spectrum solar H₂ production. *AIChE J* 2020;66:e17008. DOI
 115. Li J, Hatami M, Huang Y, Luo B, Jing D, Ma L. Efficient photothermal catalytic hydrogen production via plasma-induced photothermal effect of Cu/TiO₂ nanoparticles. *Int J Hydrog Energy* 2023; 48:6336-45. DOI
 116. Subramanyam P, Meena B, Suryakala D, Deepa M, Subrahmanyam C. Plasmonic nanometal decorated photoanodes for efficient photoelectrochemical water splitting. *Catal Today* 2021;379:1-6. DOI
 117. Wu J, Xu X, Guo X, Xie W, Pan L, Chen Y. Polypyrrole modification on BiVO₄ for photothermal-assisted photoelectrochemical water oxidation. *J Chem Phys* 2023;158:091102. DOI PubMed
 118. Zhao M, Chen T, He B, et al. Photothermal effect-enhanced photoelectrochemical water splitting of a BiVO₄ photoanode modified with dual-functional polyaniline. *J Mater Chem A* 2020;8:15976-83. DOI
 119. Xu W, Meng L, Tian W, Li S, Cao F, Li L. Polypyrrole serving as multifunctional surface modifier for photoanode enables efficient photoelectrochemical water oxidation. *Small* 2022;18:2105240. DOI
 120. Hu C, Dai L. Carbon-based metal-free catalysts for electrocatalysis beyond the ORR. *Angew Chem Int Ed* 2016;55:11736-58. DOI PubMed
 121. Li T, Guo Z, Ruan M, Zou Y, Liu Z. Doping regulating spontaneous polarization and pyroelectric effects to synergistically promote the water splitting efficiency of niobate (K_xNa_{1-x}NbO₃) pyro-photo-electrical coupling system. *Appl Surf Sci* 2022;592:153255. DOI
 122. Moon HK, Lee SH, Choi HC. In vivo near-infrared mediated tumor destruction by photothermal effect of carbon nanotubes. *ACS Nano* 2009;3:3707-13. DOI PubMed
 123. Wang Y, Chen D, Zhang J, et al. Charge relays via dual carbon-actions on nanostructured BiVO₄ for high performance photoelectrochemical water splitting. *Adv Funct Mater* 2022;32:2112738. DOI
 124. Hu XQ, Huang J, Zhao FF, et al. Photothermal effect of carbon quantum dots enhanced photoelectrochemical water splitting of hematite photoanodes. *J Mater Chem A* 2020;8:14915-20. DOI
 125. Cai J, Tang X, Liu C, et al. Bifunctional photothermal effect to promote band bending and water oxidation kinetics for improving photoelectrochemical water splitting. *Sol Energy Mater Sol Cells* 2023;257:112360. DOI
 126. Noureen L, Xie Z, Hussain M, et al. BiVO₄ and reduced graphene oxide composite hydrogels for solar-driven steam generation and decontamination of polluted water. *Sol Energy Mater Sol Cells* 2021;222:110952. DOI
 127. Wu Y, Sun Y, Fu W, et al. Graphene-based modulation on the growth of urchin-like Na₂Ti₃O₇ microspheres for photothermally enhanced H₂ generation from ammonia borane. *ACS Appl Nano Mater* 2020;3:2713-22. DOI
 128. Fang J, Sun F, Kheradmand A, et al. Solar thermo-photo catalytic hydrogen production from water with non-metal carbon nitrides. *Fuel* 2023;353:129277. DOI
 129. Wang M, Wan Z, Li Z, et al. Full spectrum solar hydrogen production by tandems of perovskite solar cells and photothermal enhanced electrocatalysts. *Chem Eng J* 2023;460:141702. DOI
 130. Qi J, Zhang W, Cao R. A new strategy for solar-to-hydrogen energy conversion: photothermal-promoted electrocatalytic water splitting. *ChemElectroChem* 2019;6:2762-5. DOI
 131. Xie X, Wang R, Ma Y, et al. Photothermal-effect-enhanced photoelectrochemical water splitting in MXene-nanosheet-modified ZnO nanorod arrays. *ACS Appl Nano Mater* 2022;5:11150-9. DOI
 132. Zhang Y, Song X, Xue S, Liang Y, Jiang H. Fabrication of hierarchically structured S-doped NiFe hydroxide/oxide electrodes for solar-assisted oxygen evolution reaction in seawater splitting. *Appl Catal A* 2023;649:118965. DOI

133. Zhang Y, Hu L, Zhang Y, Wang X, Wang H. Snowflake-Like $\text{Cu}_2\text{S}/\text{MoS}_2/\text{Pt}$ heterostructure with near infrared photothermal-enhanced electrocatalytic and photoelectrocatalytic hydrogen production. *Appl Catal B* 2022;315:121540. DOI
134. Cao A, Sang L, Yu Z, et al. Investigation of the local photothermal effects by fabricating a CQDs/Au/TiO₂ photoelectrode in a PEC water splitting system. *Catal Sci Technol* 2022;12:1859-68. DOI
135. Zhao Y, Sang L, Wang C. Thermoplasmonics effect of Au-rGO/TiO₂ photoelectrode in solar-hydrogen conversion. *Sol Energy Mater Sol Cells* 2023;255:112306. DOI
136. Landman A, Halabi R, Dias P, et al. Decoupled photoelectrochemical water splitting system for centralized hydrogen production. *Joule* 2020;4:448-71. DOI
137. Pareek A, Dom R, Borse PH. Fabrication of large area nanorod like structured CdS photoanode for solar H₂ generation using spray pyrolysis technique. *Int J Hydrog Energy* 2013;38:36-44. DOI
138. Vilanova A, Dias P, Azevedo J, et al. Solar water splitting under natural concentrated sunlight using a 200 cm² photoelectrochemical-photovoltaic device. *J Power Sources* 2020;454:227890. DOI
139. Song R, Luo B, Geng J, Song D, Jing D. Photothermocatalytic hydrogen evolution over Ni₂P/TiO₂ for full-spectrum solar energy conversion. *Ind Eng Chem Res* 2018;57:7846-54. DOI
140. Hu S, Geng J, Jing D. Photothermal effect promoting photocatalytic process in hydrogen evolution over graphene-based nanocomposite. *Top Catal* 2021. DOI
141. Gao M, Connor PKN, Ho GW. Plasmonic photothermic directed broadband sunlight harnessing for seawater catalysis and desalination. *Energy Environ Sci* 2016;9:3151-60. DOI
142. Hu S, Shi J, Luo B, Ai C, Jing D. Significantly enhanced photothermal catalytic hydrogen evolution over Cu₂O-rGO/TiO₂ composite with full spectrum solar light. *J Colloid Interface Sci* 2022;608:2058-65. DOI
143. Zhang L, Zhang X, Mo H, et al. Synergistic modulation between non-thermal and thermal effects in photothermal catalysis based on modified In₂O₃. *ACS Appl Mater Interfaces* 2023;15:39304-18. DOI
144. Ding L, Li K, Li J, et al. Integrated coupling utilization of the solar full spectrum for promoting water splitting activity over a CIZS semiconductor. *ACS Nano* 2023;17:11616-25. DOI
145. Han H, Meng X. Hydrothermal preparation of C₃N₄ on carbonized wood for photothermal-photocatalytic water splitting to efficiently evolve hydrogen. *J Colloid Interface Sci* 2023;650:846-56. DOI PubMed
146. Li J, Ding L, Su Z, et al. Non-lignin constructing the gas-solid interface for enhancing the photothermal catalytic water vapor splitting. *Adv Mater* 2023;35:e2305535. DOI
147. Wu Z, Li C, Li Z, et al. Niobium and titanium carbides (MXenes) as Superior photothermal supports for CO₂ photocatalysis. *ACS Nano* 2021;15:5696-705. DOI
148. Zhang J, Li M, Tan X, et al. Confined FeNi alloy nanoparticles in carbon nanotubes for photothermal oxidative dehydrogenation of ethane by carbon dioxide. *Appl Catal B* 2023;339:123166. DOI
149. Zhang J, Xie K, Jiang Y, et al. Photoinducing different mechanisms on a Co-Ni bimetallic alloy in catalytic dry reforming of methane. *ACS Catal* 2023;13:10855-65. DOI
150. Huang Y, Hu H, Wang S, Balogun M, Ji H, Tong Y. Low concentration nitric acid facilitate rapid electron-hole separation in vacancy-rich bismuth oxyiodide for photo-thermo-synergistic oxidation of formaldehyde. *Appl Catal B* 2017;218:700-8. DOI
151. Huang Y, Lu Y, Lin Y, et al. Cerium-based hybrid nanorods for synergetic photo-thermocatalytic degradation of organic pollutants. *J Mater Chem A* 2018;6:24740-7. DOI
152. Xiong R, Tang C, Li K, et al. Plasmon photothermal-promoted solar photocatalytic hydrogen production over a CoCr₂O₄/g-C₃N₄ heterojunction. *J Mater Chem A* 2022;10:22819-33. DOI
153. Lin Z, Gao Q, Diao P. Promoting the electrocatalytic oxygen evolution reaction on NiCo₂O₄ with infrared-thermal effect: a strategy to utilize the infrared solar energy to reduce activation energy during water splitting. *J Colloid Interface Sci* 2023;638:54-62. DOI PubMed
154. Dong B, Li F, Feng S. A visible-IR responsive BiVO₄/TiO₂ photoanode with multi-effect point defects for photothermal enhancement of photoelectrochemical water splitting. *Chem Commun* 2022;58:1621-4. DOI
155. Zhang H, Lu Y, Han W, Zhu J, Zhang Y, Huang W. Solar energy conversion and utilization: towards the emerging photo-electrochemical devices based on perovskite photovoltaics. *Chem Eng J* 2020;393:124766. DOI
156. Kim S, Piao G, Han DS, Shon HK, Park H. Solar desalination coupled with water remediation and molecular hydrogen production: a novel solar water-energy nexus. *Energy Environ Sci* 2018;11:344-53. DOI
157. Cai H, Li L, Ni H, Xiao G, Yue Z, Jiang F. GeSe-based photovoltaic thin film photoelectrode for natural seawater desalination. *Sep Purif Technol* 2023;318:124034. DOI
158. Kim YJ, Hong H, Yun J, Kim SI, Jung HY, Ryu W. Photosynthetic nanomaterial hybrids for bioelectricity and renewable energy systems. *Adv Mater* 2021;33:e2005919. DOI
159. Zhou Y, Ma Y, Wang X, et al. Leaf-structure-inspired through-hole electrode with boosted mass transfer and photothermal effect for oxygen evolution reactions. *Adv Funct Mater* 2023;33:2304296. DOI
160. Zhang B, Luo H, Ai B, et al. Modulating surface electron density of heterointerface with bio-inspired light-trapping nano-structure to boost kinetics of overall water splitting. *Small* 2023;19:e2205431. DOI